

Nonreciprocal electrical transport in linear systems with balanced gain and loss in the bulk

Rupak Bag and Dibyendu Roy
Raman Research Institute, Bengaluru 560080, India

We investigate electrical transport in a quantum wire of N sites connected to an equal number ($N_i/2$) of sources and drains of charges in bulk. Each source and drain injects and extracts charges at the same rate, respectively. We show that the linear-response electrical current is nonreciprocal in such a system when the arrangement of sources and drains breaks the system's parity. We prove that inelastic scattering is essential for nonreciprocity in this system. For this, we invoke a master equation description of classical charge transport in a similar system. The nonreciprocal current in quantum wire matches that in the classical model for $N_i/N \sim 1$, generating a finite scattering length much smaller than the length of the wire. The nonreciprocity in the quantum wire oscillates with wire length when $N_i/N \ll 1$, and it can vanish at specific lengths.

Charge transport in matters has a long history, starting from empirical law by Ohm in the early days to kinetic equation description by Drude to recent fully quantum transport analysis pioneered by Landauer and Büttiker [1–3]. Even today, electrical transport is one of the most important research topics for practical applications and basic understanding [4–14]. Here, we revisit an intriguing problem of charge transport in an open one-dimensional (1D) system, which is connected to the alternative sources (S's) and drains (D's) of charges in the middle. These sources and drains lead to the gain and loss of particles and energies in the system. The role of balanced gain and loss of particles or energies has been extensively investigated in recent years in the context of an effective parity-time \mathcal{PT} symmetry in classical and quantum systems [15–22]. We examine the role of balanced injection and extraction of particles from a wire in classical and quantum transport regimes.

Let us consider a wire of length L and resistance R , which is biased by voltage V at the boundaries as shown in the inset of Fig. 1(a). The wire is further connected to a current S and a D at $L/3$ distance from the left and the right boundary, respectively. The S (D) injects (draws) an electric current I_g in (from) the wire. The electric current flowing in (I_{in}) and out (I_{out}) at the boundaries of the wire can be calculated easily following the Ohm's or Kirchhoff's circuit law, and it is $I_{\text{in}} = I_{\text{out}} = (V/R - I_g/3)$ for a forward bias ($V > 0$). The current values change to $(V/R + I_g/3)$ for a reverse bias ($V < 0$). Thus, the charge transport through the wire in the presence of balanced gain and loss of charges from the S and D is nonreciprocal. The presence of S and D breaks the parity of the wire, which leads to the nonreciprocity in the current response. Nevertheless, it is not clear what the physical mechanism/origin of the current nonreciprocity is. We seek to understand the mechanism in classical and quantum transport processes. We particularly reveal that the nonreciprocity in linear-response transport emerges for a finite rate of gain and loss in such systems in the presence of inelastic scattering and parity-breaking due to the sources and drains.

We first invoke a master equation description (inspired by the Drude model) of charge (e) transport with two species of right- and left-moving charges [23]. Consider a 1D lattice model with N sites and lattice spacing a . We take $N_i/2 \equiv (N/2 - 1)$ dimers of a pair of S and D connected to the bulk sites of the lattice. Each such S (D) is again injecting (extracting) I_g charge current in (from) the system. We

take $\rho^\pm(x)$ as the density of the right- and left-movers at position x on the lattice. In bulk, these right- and left-movers hop with probability p to the next site in the right and left direction, respectively. They can also convert between themselves with a finite probability $(1-p)$ at the connection points of the sources and drains with the lattice. In addition, the presence of S (D) current I_g at position x increases (reduces) the density of the left and the right movers by an amount of $I_g\tau/(2ea)$. To generate a bias across the system similar to the voltage difference, we connect the two ends of the lattice to two reservoirs. Thus, we set the density of particles inside the reservoirs as $\rho^\pm(x=0) = \rho_0 + \delta\rho$ at the left terminal, and $\rho^\pm(x=(N+1)a) = \rho_0$ at the right terminal for a forward bias. For the reverse biasing, we switch the densities at two terminals. We then write discrete time-evolution equation for the density fields $\rho^\pm(x,t)$ in time steps τ as

$$\rho^+(a,t+\tau) - \rho^+(a,t) = \rho^+(0,t) - \rho^+(a,t), \quad (1)$$

$$\rho^-(a,t+\tau) - \rho^-(a,t) = p\rho^-(2a,t) - \rho^-(a,t), \quad (2)$$

$$\begin{aligned} \rho^\pm(x,t+\tau) - \rho^\pm(x,t) &= p[\rho^\pm(x \mp a,t) - \rho^\pm(x,t)] \\ &\quad - \frac{p-1}{2}[(1 \pm 1)\delta_{x,2a} + (1 \mp 1)\delta_{x,(N-1)a}]\rho^\pm(x \mp a,t) \\ &\quad + (1-p)[\rho^\mp(x,t) - \rho^\pm(x,t)] + (-1)^{\frac{x}{a}} \frac{I_g\tau}{2ea}, \end{aligned} \quad (3)$$

$$\rho^+(Na,t+\tau) - \rho^+(Na,t) = p\rho^+(L,t) - \rho^+(Na,t), \quad (4)$$

$$\rho^-(Na,t+\tau) - \rho^-(Na,t) = \rho^-(L+2a,t) - \rho^-(Na,t), \quad (5)$$

where $x \in [2a, L]$, $L = (N-1)a$ and $\delta_{x,x'}$ is the Kronecker-delta symbol. We set the left-hand side of Eqs. (1-5) to zero in the steady state of the system at long times. We immediately find $\rho^+(a,t) = \rho_0 + \delta\rho$ and $\rho^-(L+a,t) = \rho_0$ for all time. We can define the steady-state charge current flowing through the two ends of the lattice by applying the continuity equations. The currents flowing in and out of the lattice are given by $I_{\text{in}} = (ea/\tau)(\rho^+(a,t) - p\rho^-(2a,t))$ and $I_{\text{out}} = (ea/\tau)(p\rho^+(L) - \rho^-(L+a))$, respectively [24]. For $N=4$, we find $\rho^\pm(x)$ by solving Eqs. 1-5, which gives $I_{\text{in}} = I_{\text{out}} = ((ea/\tau)\delta\rho - (1-p)I_g)/(3-2p)$. These current values change to $((ea/\tau)\delta\rho + (1-p)I_g)/(3-2p)$ for the reverse bias. Thus, I_{in} matches with the previous result of the circuit model in the limit $p \rightarrow 0$, when we identify group velocity $v_F = a/\tau$ and $ev_F\delta\rho/3 = V/R$. The limit $p \rightarrow 0$ signals a large inter-conversion between left- and right-movers at each

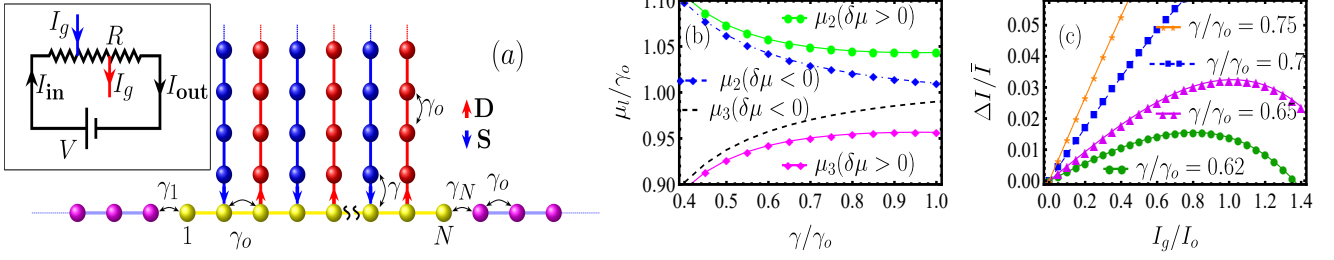


FIG. 1: (a) Schematic of an open quantum wire (yellow dots) connected to multiple sources (S's) and drains (D's) in the middle. Inset shows a resistive model with a pair of S and D. (b) Variation of chemical potentials μ_2 and μ_3 with γ in the linear response regime of a short quantum wire ($N = 4$) with a pair of S and D, where $\bar{\mu}/\gamma_0 = 1$, $I_g/I_0 = 0.3$. (c) Relative current nonreciprocity, $\Delta I/\bar{I}$ with increasing I_g beyond linear response regime of a short wire ($N = 4, N_i = 2$). Here, $\Delta I = |I_1(\delta\mu < 0)| - |I_1(\delta\mu > 0)|$, $2\bar{I} = |I_1(\delta\mu > 0)| + |I_1(\delta\mu < 0)|$, and $\bar{\mu}/\gamma_0 = 1.52$. In plots (b-c), we fix $\delta\mu/\gamma_0 = 0.1$ and $\delta\mu/\gamma_0 = -0.1$ for forward and reverse bias, respectively, with $e = 1$.

connection between S or D and the lattice. The above nonreciprocity in current flow disappears in the opposite limit of $p \rightarrow 1$ for such a short lattice with only one pair of S and D. Thus, the conversion between two species of charge carriers is the physical origin of nonreciprocal transport in this system in the presence of S and D. The inter-conversion also leads to resistance in such classical transport channel.

We next take an extended lattice with a large number ($N_i \gg 2$) of S and D. We now solve a large set of linear coupled equations for $\rho^\pm(x)$ at the steady state of the lattice with the boundary conditions of $\rho^+(a, t) = \rho_0 + \delta\rho$ and $\rho^-(L+a, t) = \rho_0$. These solutions for densities of both the species at odd and even sites are [24]

$$\begin{aligned} \rho^-(x) &= \frac{\bar{\rho} - (2p-1)I_g/(2ev_F)}{p(1+(N-2)(1-p))}, \quad x = 3a, 5a, \dots, L, \\ \rho^-(x) &= \frac{\bar{\rho} + N(1-p)I_g/(2ev_F)}{p(1+(N-2)(1-p))}, \quad x = 2a, 4a, \dots, L-a, \\ \rho^+(x) &= \rho^-(x) + \frac{\delta\rho + I_g/(2ev_F)}{1+(N-2)(1-p)}, \quad x = 2a, 3a, \dots, L, \\ \bar{\rho} &= \rho_0 + [(N-2)\rho_0 + N\delta\rho - \frac{x}{a}(\delta\rho + \frac{I_g}{2ev_F})](1-p). \end{aligned} \quad (6)$$

We insert these densities in I_{in} and I_{out} to find the steady-state charge current at the boundaries as [24]

$$I_{\text{in}} = I_{\text{out}} = \frac{ev_F \delta\rho - (1-p)(N/2-1)I_g}{1+(N-2)(1-p)}. \quad (7)$$

When the densities of the species at the two terminals are reversed, the value of I_{in} and I_{out} is not the same as before for a non-zero I_g as long as $1-p > 0$. Hence, we reaffirm that we need a finite inter-conversion of species to get nonreciprocity. We further define a length scale $l_c = a/(1-p)$, which we later identify as the scattering length that emerged due to the inter-conversion of species. Then, we can rewrite Eq. 7 as

$$I_{\text{in}} = I_{\text{out}} = \frac{ev_F \delta\rho}{1+L/l_c} - \frac{I_g}{2} \left(1 - \frac{1}{1+L/l_c} \right), \quad (8)$$

where we assume $(N-2)a \approx L$ for $N \gg 2$. Thus, we find the emergence of a finite l_c is an essential entity for nonreciprocity as nonreciprocity vanishes for $l_c \rightarrow \infty$. Till now, we have

discussed transport in classical channels without quantum coherence. It is also exciting how quantum coherence competes with nonreciprocity. For this, we now turn to charge transport in quantum channels.

A full-fledged quantum transport analysis generalizing approach of Landauer and Büttiker [1–3] requires quantum transport channel(s) connected to baths at the boundaries generating a voltage bias [23, 25–28]. We consider a finite-length tight-binding (TB) wire of spinless fermions connected to two microscopic bath models at two ends. The baths are kept at different chemical potentials to create a voltage difference across the wire. We further model the sources and drains as microscopic baths whose chemical potentials are fixed self-consistently so that they inject or draw the required current I_g to the transport channel [23, 29–36]. All the microscopic baths are modeled as semi-infinite TB chains, and all the baths are kept at the same temperature T for simplicity of the analytical calculation.

The Hamiltonian of the full system, depicted in Fig. 1(a), consisting of the wire plus all the baths, is given by $\hat{H} = \hat{H}_w + \sum_{l=1}^N (\hat{H}_B^l + \hat{V}^l)$, where (setting $\hbar = 1$)

$$\hat{H}_w = -\gamma_0 \sum_{l=1}^{N-1} (\hat{c}_l^\dagger \hat{c}_{l+1} + \hat{c}_{l+1}^\dagger \hat{c}_l), \quad (9)$$

$$\hat{H}_B^l = -\gamma_0 \sum_{m=1}^{\infty} (\hat{b}_m^\dagger(l) \hat{b}_{m+1}(l) + \hat{b}_{m+1}^\dagger(l) \hat{b}_m(l)), \quad (10)$$

$$\hat{V}^l = -\gamma (\hat{b}_1^\dagger(l) \hat{c}_l + \hat{c}_l^\dagger \hat{b}_1(l)). \quad (11)$$

Here, \hat{H}_w describes a 1D quantum wire of N sites. The operator \hat{c}_l^\dagger (\hat{c}_l) creates (annihilates) a spinless fermion at site l , and it can hop to two neighboring sites with an amplitude γ_0 . \hat{H}_B^l denotes the Hamiltonian of the bath connected to site l of the wire. Here, $\hat{b}_m^\dagger(l)$ ($\hat{b}_m(l)$) creates (annihilates) a spinless fermion at site m inside a bath. We set the hopping amplitude within each TB bath also γ_0 . The coupling Hamiltonian between l^{th} site of the wire and a bath is \hat{V}^l , and γ is the related coupling amplitude. The chemical po-

tential of the left and right bath connected to site $l = 1, N$, respectively, are fixed to be μ_L and μ_R . The average and the difference of the left and right bath's chemical potentials are $\bar{\mu} = (\mu_L + \mu_R)/2$ and $\delta\mu = \mu_L - \mu_R$, respectively. The chemical potential $\{\mu_l | l = 2, 3, \dots, N-1\}$ of the middle baths are determined self-consistently to get I_g current injected (drawn) by the S (D) bath at an even (odd) site in the bulk of the wire. We further set $\gamma_l = \gamma$ for $l = 2, \dots, N-1$ and $\gamma_o = 1$, allowing all the coupling and hopping amplitudes to be chosen in the units of γ_o .

Let us assume that the baths are connected to the wire in the remote past $t_o \rightarrow -\infty$. Following the method in [23, 27, 28], we get generalized quantum Langevin equations for the wire operators for site $l = 1, 2, 3, \dots, N$ as [24]

$$i\frac{\partial \hat{c}_l}{\partial t} = -(\hat{c}_{l+1} + \hat{c}_{l-1}) + \int_{-\infty}^t d\tau \Sigma_l^+(t-\tau) \hat{c}_l(\tau) + \hat{\eta}_l(t), \quad (12)$$

where the noise $\hat{\eta}_l(t) = -i\gamma_l \sum_m g_{1,m}^+(l, t-t_o) \hat{b}_m(l, t_o)$ and the self-energy correction $\Sigma_l^+(t) = \gamma_l^2 g_{1,1}^+(l, t)$ generate fluctuation and dissipation in the wire due to its coupling with the bath at l^{th} site. The open boundary condition on the wire gives $\hat{c}_0 = \hat{c}_{N+1} = 0$. Here, $\hat{g}^+(l, t) = -i\theta(t)e^{-i\hat{H}_b^l t}$ is single-particle retarded Green's function of the bath at l^{th} site and $\theta(t)$ is the Heaviside step function.

When the wire attains a steady state at a long time, we can utilize the Fourier transform method [27] to write the steady-state solution of Eq. 12 as $\hat{c}_l(\omega) = \sum_{l'=1}^N G_{ll'}^+(\omega) \hat{\eta}_{l'}(\omega)$, where $\hat{c}_l(\omega) = \int_{-\infty}^{\infty} dt e^{i\omega t} \hat{c}_l(t)/(2\pi)$, $\hat{\eta}_l(\omega) = \int_{-\infty}^{\infty} dt e^{i\omega t} \hat{\eta}_l(t)/(2\pi)$, and $\Sigma_l^+(\omega) = \int_{-\infty}^{\infty} dt e^{i\omega t} \Sigma_l^+(t)$. Here, $\hat{G}^+(\omega)$ is the Green's function of the full system. It can be written as $\hat{G}^+(\omega) = (\omega - \hat{H}_w - \hat{\Sigma}^+(\omega))^{-1}$ for its elements on the wire, where the elements of $\hat{\Sigma}^+$ are $\Sigma_{ll'}^+(\omega) = \Sigma_l^+(\omega) \delta_{ll'}$. The noise properties in the frequency domain are the following: $\langle \hat{\eta}_l(\omega) \rangle = 0$ and $\langle \hat{\eta}_l^\dagger(\omega) \hat{\eta}_{l'}(\omega') \rangle = \gamma_l^2 f_l(\omega) \rho_l(\omega) \delta(\omega - \omega') \delta_{ll'}$, where $f_l(\omega) = 1/(e^{(\omega - \mu_l)/k_B T} + 1)$ is the Fermi distribution function and $\rho_l(\omega) = \sqrt{4 - \omega^2}/(2\pi)$ is the local density of states at the first site of the l^{th} bath. Here, $\langle \dots \rangle$ denotes averaging over the grand-canonical distribution of the baths. We apply the continuity equations for the local density of particles $n_l = \langle \hat{c}_l^\dagger \hat{c}_l \rangle$ to define two kinds of charge currents in the system: (i) $I_l = ie\gamma_l \langle \hat{c}_l^\dagger \hat{b}_1(l) - \hat{b}_1^\dagger(l) \hat{c}_l \rangle$, which is the current flowing from the bath at l^{th} site to that site of the wire, and (ii) $J_l = ie \langle \hat{c}_{l+1}^\dagger \hat{c}_l - \hat{c}_l^\dagger \hat{c}_{l+1} \rangle$ for $l = 1, 2, \dots, N-1$ denotes the current flowing from site l to site $l+1$ inside the wire. We use the noise properties to obtain the average currents. To perform analytical calculation, we additionally assume a linear-response regime with small chemical potential biases about $\bar{\mu}$: $\delta\mu \ll \bar{\mu}$ and $\delta\mu_l = \mu_l - \bar{\mu} \ll \bar{\mu}$ for $l = 2, 3, \dots, N-1$. This simplifies the average current expressions in the steady state as follows [24]: $I_l = \frac{e}{2\pi} \sum_{l'=1}^N \mathcal{T}_{ll'}(\mu_l - \mu_{l'})$ and $J_l = \frac{e}{2\pi} \sum_{l'=1}^N \mathcal{F}_{ll'}(\mu_l - \mu_{l'})$, where the different transmission coefficients are $\mathcal{T}_{ll'} = 4\pi^2 \gamma_l^2 \gamma_{l'}^2 \rho_l(\bar{\mu}) \rho_{l'}(\bar{\mu}) |G_{ll'}^+(\bar{\mu})|^2$ and $\mathcal{F}_{ll'} = 2i\pi \gamma_l^2 \gamma_{l'}^2 \rho_l(\bar{\mu}) (G_{ll'}^{+*}(\bar{\mu}) G_{l+1l'}^+(\bar{\mu}) - G_{l+1l'}^{+*}(\bar{\mu}) G_{ll'}^+(\bar{\mu}))$. We find μ_l of the middle baths from the self-consistency condition

that $I_l = (-1)^l I_g$ for $l = 2, 3, \dots, N-1$. We further set $\gamma_l/\gamma_o = \gamma_N/\gamma_o = 1$, which leads to transparent (reflection-less) contacts for the two ends of the wire [26]. We denote $I_o = e\delta\mu/(2\pi)$ as the corresponding reflection-less ballistic current within the wire when $\gamma = 0$.

We first consider the case with $N = 4$, where the wire contains a single S-D dimer. The chemical potentials of the middle baths are obtained as $\mu_2 = \bar{\mu} + \Delta_\mu$ and $\mu_3 = \bar{\mu} - \Delta_\mu$ (Fig.1(b)), where

$$\Delta_\mu = \frac{\pi \mathcal{D}(\bar{\mu}) I_g / e + \gamma^4 (1 - \bar{\mu}^2 / 4) (\gamma^2 + 2 - \bar{\mu}^2) \delta\mu}{2\gamma^2 (1 - \bar{\mu}^2 / 4) (2 + \gamma^4 + 4\gamma^2 - \gamma^2 \bar{\mu}^2)}, \quad (13)$$

and $\mathcal{D}(\bar{\mu}) = (2 + 2\gamma^2 + \gamma^4)^2 - (1 + 2\gamma^2 + 5\gamma^4 + 2\gamma^6) \bar{\mu}^2 + \gamma^4 \bar{\mu}^4$. By expanding Δ_μ in the powers of γ^2 , we get $\Delta_\mu = \pi I_g / (e\gamma^2) + \pi \bar{\mu}^2 I_g / (2e) + \mathcal{O}(\gamma^2)$. Thus, I_g cannot be arbitrarily large for a small γ for the system to be in a linear-response regime, e.g., $\Delta_\mu \leq \delta\mu$, which restricts $I_g \leq 2\gamma^2 I_o$ when $\gamma/\gamma_o \ll 1$.

At long-time steady state of the wire, the charge current at the left and right boundaries for a non-zero $\delta\mu$ are related as $I_1 = -I_4$, which can be expressed as $I_1 = G_4(\delta\mu/e) - \delta I$ [24], where

$$G_4 \approx \frac{e^2}{2\pi} (1 - \gamma^2), \quad \delta I \approx \gamma^2 (2 - \bar{\mu}^2) \frac{I_g}{2}, \quad (14)$$

for $\gamma/\gamma_o \ll 1$. Thus, the magnitude of I_1 for the forward bias ($\delta\mu > 0$) is different from that for the reverse bias ($\delta\mu < 0$) when $I_g \neq 0$. This leads to nonreciprocal charge transport in the wire in the presence of a pair of source and drain, as discussed earlier for the two previous models. The value for the nonreciprocity once again becomes $2I_g/3$ when $\gamma^2 = (\bar{\mu}^2 - 1 + \sqrt{5 - 2\bar{\mu}^2 + \bar{\mu}^4})/2$ in the non-perturbative regime [24]. The relative nonreciprocity in the linear response regime is given by $2e\delta I/(G_4\delta\mu)$, which grows linearly with I_g . Interestingly, the relative nonreciprocity behaves differently at larger I_g in the nonlinear response regime [24] as shown in Fig. 1(c).

Next, we discuss charge transport in a longer wire ($N \gg 4$) with $(N/2 - 1)$ S-D dimers connected to the middle sites. For $\gamma < 1$ and $N \gg 4$, we self-consistently determine μ_l of the S's and D's in the middle as [24]

$$\mu_l = \mu_L - \phi + \left[\frac{l_c}{2\sigma} + (-1)^l \nabla \right] \frac{eI_g}{2} - 2\frac{\phi}{l_c} (l-2), \quad (15)$$

$$\phi = \frac{\delta\mu + eI_g l_c / (2\sigma)}{2[1 + (N-3)/l_c]}, \quad \text{and} \quad \nabla = \frac{\coth^2 \alpha_R}{2\sigma}, \quad (16)$$

for $l = 2, 3, \dots, N-1$. Here, we define the scattering length $l_c = 1/\alpha_R$ and the electrical conductivity $\sigma = e^2 \sin^2 \alpha_l \coth \alpha_R / (2\pi |\sinh \alpha|^2)$. Further, α_R and α_l are, respectively, the real and imaginary parts of the complex-valued function $\alpha = \log_e [\mathcal{C} + \sqrt{\mathcal{C}^2 - 1}]$ with $\alpha_R > 0$ and $2\mathcal{C} = \bar{\mu} - \gamma^2 (\bar{\mu} - i\sqrt{4 - \bar{\mu}^2})/2$. We show μ_l over the wire sites l for $I_g \neq 0$ in Fig. 2(a), where we depict an excellent match between the analytical expression of μ_l (Eq. 81) with exact numerical results for a fixed N and γ . Due to local injection and extraction of particles by the S and D, the charge

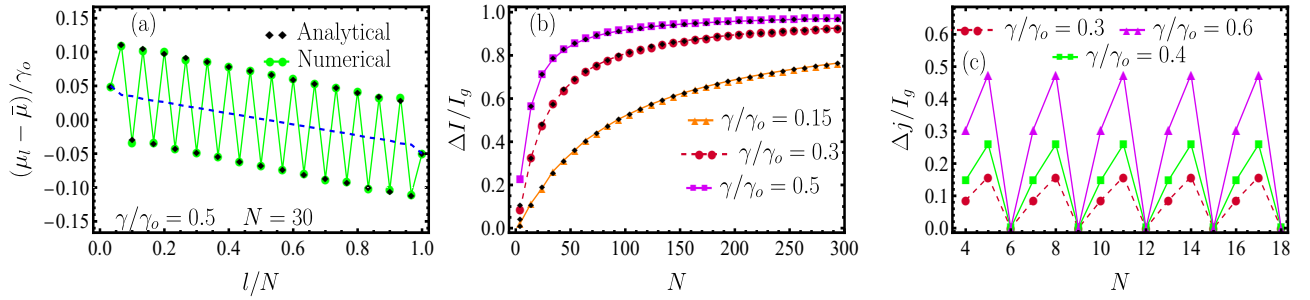


FIG. 2: (a) Chemical potential profile in a long quantum wire ($N = 30$) connected to $N_i/2 = N/2 - 1$ number of S-D dimers. Parameters are $\bar{\mu}/\gamma_0 = 1.4$, $I_g/I_o = 0.3$. The Blue dashed line shows the corresponding plot for $I_g = 0$ with $\gamma \neq 0$. (b) Variation of current nonreciprocity $\Delta I = |I_1(\delta\mu < 0)| - |I_1(\delta\mu > 0)|$, with N in a long wire with $N_i/2 = N/2 - 1$ number of S-D dimers. Here, $I_g/I_o = 0.05$, and $\bar{\mu}/\gamma_0 = 1.0$. The black dots represent the corresponding analytical points obtained using $2\delta J$ in Eq. (17). (c) Periodic variation of current nonreciprocity, Δj with N in a quantum wire with only one S-D dimer ($N_i = 2$). Here, $I_g/I_o = 0.1$, and $\bar{\mu}/\gamma_0 = 1.0$. In all the plots (a-c), we fix $\delta\mu/\gamma_0 = 0.1$ and $e = 1$.

current J_l at an even and an odd site of the wire are not the same, and we call them by J_S and J_D , respectively. Applying μ_l from Eq. (81) in J_l , we find J_D and J_S for $N \gg 4$ as $J_D = G_N(\delta\mu/e) - \delta J$ and $J_S = J_D + I_g$, where

$$G_N = \frac{\sigma}{l_c + N - 3}, \quad \delta J = \frac{I_g}{2} \left(1 - \frac{l_c}{l_c + N - 3} \right). \quad (17)$$

We observe $J_D = I_1 = -I_N$ from the continuity equation at steady state. Thus, the particle current at the left and right junction between the wire and respective baths are J_D . We further observe that I_1 or I_N is again different for forward ($\delta\mu > 0$) and reverse bias ($\delta\mu < 0$). The value of nonreciprocity in charge current is $2\delta J$, which matches that obtained within the master equation analysis. Coupling of S and D baths to all middle sites of the wire generates inelastic scattering for the charge carriers, which leads to loss of coherence and energy dissipation (Joule heating). These scatterings give rise to a large resistance in the wire against particle transport, and the resistance itself depends on the length of the wire. Thus, we find an emergent nonreciprocal Drude-type transport in the quantum wire in the presence of S and D baths to all middle sites. We can further relate the inelastic scattering due to the S and D baths in quantum channels to the inter-conversion of species in classical channels from the similarities of Eq. 17 and Eq. 8, when we identify $\sigma(\delta\mu/e)$ with $ev_F\delta\rho l_c$.

The emergence of l_c due to the coupling of the wire with middle baths leads to two regimes of quantum transport depending on N and l_c . When $N \gg l_c$ for a long wire with a finite γ , we observe that δJ can be approximated as $I_g/2$, which gives $J_D = G_N(\delta\mu/e) - I_g/2$, $J_S = G_N(\delta\mu/e) + I_g/2$ and the nonreciprocity $2\delta J = I_g$. On the contrary, when $N \ll l_c$, we get the nonreciprocity $2\delta J \approx \gamma^2(N-3)I_g/2$ by approximating $l_c = \alpha_R^{-1} \approx 2/\gamma^2$, $\sigma \approx e^2 l_c / (2\pi)$ and $\nabla \approx \pi l_c / e^2$ for $\gamma \ll 1$. In Fig. 2(b), we display two different regimes of nonreciprocity by plotting $2\delta J$ with N . It shows a linear growth of $2\delta J$ with N for shorter $N (\ll l_c)$ and saturation to I_g at longer N .

The coherence in charge transport through the long quantum wire is severely suppressed when all middle sites of the long wire are connected to S and D baths. However, it plays a vital role in transport when we connect some or only two middle sites to the S and D baths. Next, we analyze how coherence controls nonreciprocity in a quantum wire. We take a quantum wire with N sites, where an S and a D bath (e.g., $N_i = 2$) are connected to the sites $l = 2$ and $N - 1$, respectively. All the $(N - 4)$ middle sites for $l = 3, 4, \dots, N - 2$ are free and form ballistic channels for charge transport. The wire is again under a finite bias $\delta\mu$ from the left and right boundary. The chemical potential of S and D baths can be derived from the requirement of I_g current injected in and extracted from the wire in the steady state. Applying those chemical potentials, we find the current I_1, I_N at the boundaries, showing nonreciprocity under reversal of voltage bias $\delta\mu$. The nonreciprocity in charge current for this case is given by $\Delta j = 2(\Xi - 1)I_g / (1 + 2\gamma^2 + \Xi)$, where [24]

$$\Xi = \frac{|(2\mathcal{A}\mathcal{C} - 1)\sin(N-3)k_F - \mathcal{A}\sin(N-4)k_F|^2}{\sin^2 k_F}, \quad (18)$$

$\mathcal{A} = \bar{\mu}/2 + i\sqrt{1 - \bar{\mu}^4}/4$, and the Fermi momentum $k_F = \cos^{-1}(\bar{\mu}/2)$, which gives Fermi wavelength $\lambda_F = 2\pi/\cos^{-1}(\bar{\mu}/2)$. We show Δj with varying N in Fig. 2(c) for $\bar{\mu} = 1$ giving $\lambda_F = 6$. We observe Δj oscillates with N for different γ , displaying an interplay between quantum coherence and nonreciprocity. Further, Δj vanishes when the length $(N - 3)$ between S and D baths is an integer multiple of $\lambda_F/2$. Then, the chemical potential of S and D remains the same for both forward and reverse voltage bias. Such oscillations and zeros of nonreciprocity do not appear in a similar set-up within the master equation analysis for classical transport channels [24].

Motivated by recent efforts to explore transport in effective $\mathcal{P}\mathcal{T}$ symmetric Hamiltonian systems [18, 19, 21, 22], we formulate a statistical description of transport in linear systems with balanced gain and loss of particles or charges in bulk. In

contrast to most studies in effective \mathcal{PT} symmetric Hamiltonian systems, our work does not require any untested assumptions in describing transport. While directional transport has been demonstrated in effective \mathcal{PT} symmetric models only in the nonlinear regime [21, 22], our study shows nonreciprocity in transport in the linear-response regime without magnetic fields [37]. The linear regime could help engineer an electrical diode or rectifier since the device operation would work irrespective of the specific form of the signal (e.g., intensity). Nonreciprocity in our explored models has some similarity to

the optical isolation accomplished by spatial-temporal refractive index modulations that simultaneously impart frequency and wavevector shifts during the photonic transition process [38]. Nevertheless, our statistical modeling in an open quantum electrical system differs from their closed optical system, e.g., the explicit presence of quantum noises in an open system [37, 39]. Finally, it would be exciting to extend our current analysis with balanced loss and gain to topological wires, e.g., the Su–Schrieffer–Heeger (SSH) chains [40, 41] and the Majorana wires [10, 11, 28].

-
- [1] P. A. Mello and N. Kumar, *Quantum Transport in Mesoscopic Systems: Complexity and Statistical Fluctuations, a Maximum-entropy Viewpoint* (Oxford University Press, Oxford, 2004).
- [2] S. Dutta, *Quantum Transport: Atom to Transistor* (Cambridge University Press, Cambridge, 2005).
- [3] E. Akkermans and G. Montambaux, *Mesoscopic Physics of Electrons and Photons* (Cambridge University Press, Cambridge, 2007).
- [4] G. Badawy and E. P. Bakkers, Electronic transport and quantum phenomena in nanowires, *Chem. Rev.* **124**, 2419 (2024).
- [5] A. M. Lord, T. G. Maffei, O. Kryvchenkova, R. J. Cobley, K. Kalna, D. M. Kepaptsoglou, Q. M. Ramasse, A. S. Walton, M. B. Ward, J. Koble, *et al.*, Controlling the electrical transport properties of nanocontacts to nanowires, *Nano Lett.* **15**, 4248 (2015).
- [6] S. Kumbhakar, T. K. Maji, B. Tongbram, S. Mandal, S. H. Soundararaj, B. Debnath, T. P. Sai, M. Jain, H. Krishnamurthy, A. Pandey, *et al.*, Engineering ultra-strong electron-phonon coupling and nonclassical electron transport in crystalline gold with nanoscale interfaces, [arXiv:2405.14684](https://arxiv.org/abs/2405.14684) (2020).
- [7] R. Dutta, A. Pradhan, P. Mondal, S. Kakkar, T. P. Sai, A. Ghosh, and J. K. Basu, Enhancing carrier diffusion length and quantum efficiency through photoinduced charge transfer in layered graphene–semiconducting quantum dot devices, *ACS Appl. Mater. Interfaces* **13**, 24295 (2021).
- [8] A. Fabian, M. Gradhand, M. Czerner, and C. Heiliger, First-principles scattering with Büttiker probes: The role of self-energies, *Phys. Rev. B* **105**, 165106 (2022).
- [9] D. Hagenmüller, J. Schachenmayer, S. Schütz, C. Genes, and G. Pupillo, Cavity-enhanced transport of charge, *Phys. Rev. Lett.* **119**, 223601 (2017).
- [10] A. E. Antipov, A. Bargerbos, G. W. Winkler, B. Bauer, E. Rossi, and R. M. Lutchyn, Effects of gate-induced electric fields on semiconductor Majorana nanowires, *Phys. Rev. X* **8**, 031041 (2018).
- [11] S. Pagano, N. Martucciello, E. Enrico, E. Monticone, K. Iida, and C. Barone, Iron-based superconducting nanowires: Electric transport and voltage-noise properties, *Nanomaterials* **10**, 862 (2020).
- [12] J. Li, K.-C. Lee, M.-H. Hsieh, S.-H. Yang, Y.-M. Chang, J.-K. Chang, C.-Y. Lin, and Y.-F. Lin, Probing charge transport difference in parallel and vertical layered electronics with thin graphite source/drain contacts, *Sci. Rep.* **9**, 20087 (2019).
- [13] S. Islam, S. Bhattacharyya, H. Nhalil, S. Elizabeth, and A. Ghosh, Signature of pseudodiffusive transport in mesoscopic topological insulators, *Phys. Rev. Res.* **2**, 033019 (2020).
- [14] M. M. Mirza, F. J. Schupp, J. A. Mol, D. A. MacLaren, G. A. D. Briggs, and D. J. Paul, One dimensional transport in silicon nanowire junction-less field effect transistors, *Sci. Rep.* **7**, 3004 (2017).
- [15] C. M. Bender and S. Boettcher, Real spectra in non-Hermitian Hamiltonians having PT symmetry, *Phys. Rev. Lett.* **80**, 5243 (1998).
- [16] A. Mostafazadeh, Pseudo-Hermiticity versus PT symmetry: The necessary condition for the reality of the spectrum of a non-Hermitian Hamiltonian, *J. Math. Phys.* **43**, 205 (2002).
- [17] C. M. Bender, M. V. Berry, and A. Mandilara, Generalized PT symmetry and real spectra, *J. Phys. A: Math. Gen.* **35**, L467 (2002).
- [18] C. E. Rüter, K. G. Makris, R. El-Ganainy, D. N. Christodoulides, M. Segev, and D. Kip, Observation of parity–time symmetry in optics, *Nat. Phys.* **6**, 192 (2010).
- [19] J. Schindler, A. Li, M. C. Zheng, F. M. Ellis, and T. Kottos, Experimental study of active LRC circuits with \mathcal{PT} symmetries, *Phys. Rev. A* **84**, 040101 (2011).
- [20] N. Bender, S. Factor, J. D. Bodyfelt, H. Ramezani, D. N. Christodoulides, F. M. Ellis, and T. Kottos, Observation of asymmetric transport in structures with active nonlinearities, *Phys. Rev. Lett.* **110**, 234101 (2013).
- [21] L. Chang, X. Jiang, S. Hua, C. Yang, J. Wen, L. Jiang, G. Li, G. Wang, and M. Xiao, Parity-time symmetry and variable optical isolation in active-passive-coupled microresonators, *Nat. Photon.* **8**, 524 (2014).
- [22] B. Peng, Ş. K. Özdemir, F. Lei, F. Monifi, M. Gianfreda, G. L. Long, S. Fan, F. Nori, C. M. Bender, and L. Yang, Parity-time-symmetric whispering-gallery microcavities, *Nat. Phys.* **10**, 394 (2014).
- [23] D. Roy and A. Dhar, Electron transport in a one dimensional conductor with inelastic scattering by self-consistent reservoirs, *Phys. Rev. B* **75**, 195110 (2007).
- [24] See Supplemental Material (SM) for detailed derivation of master equation description for classical transport channels and quantum langevin equation method for open quantum wires.
- [25] H. Bruus and K. Flensberg, *Many-Body Quantum Theory in Condensed Matter Physics : An Introduction* (Oxford University Press, Oxford, 2004).
- [26] A. Dhar and B. Sriram Shastry, Quantum transport using the Ford-Kac-Mazur formalism, *Phys. Rev. B* **67**, 195405 (2003).
- [27] A. Dhar and D. Sen, Nonequilibrium Green’s function formalism and the problem of bound states, *Phys. Rev. B* **73**, 085119 (2006).
- [28] N. Bondyopadhyaya and D. Roy, Nonequilibrium electrical, thermal and spin transport in open quantum systems of topological superconductors, semiconductors and metals, *J. Stat. Phys.* **187**, 11 (2022).
- [29] M. Büttiker, Small normal-metal loop coupled to an electron reservoir, *Phys. Rev. B* **32**, 1846 (1985).
- [30] M. Büttiker, Role of quantum coherence in series resistors,

- [Phys. Rev. B **33**, 3020 \(1986\)](#).
- [31] J. L. D'Amato and H. M. Pastawski, Conductance of a disordered linear chain including inelastic scattering events, [Phys. Rev. B **41**, 7411 \(1990\)](#).
- [32] A. Dhar and D. Roy, Heat transport in harmonic lattices, [J. Stat. Phys. **125**, 801 \(2006\)](#).
- [33] D. Roy, Electron transport in an open mesoscopic metallic ring, [J. Phys. Condens. Matter **20**, 025206 \(2007\)](#).
- [34] D. Roy, Crossover from ballistic to diffusive thermal transport in quantum Langevin dynamics study of a harmonic chain connected to self-consistent reservoirs, [Phys. Rev. E **77**, 062102 \(2008\)](#).
- [35] M. Kulkarni, K. L. Tiwari, and D. Segal, Full density matrix dynamics for large quantum systems: interactions, decoherence and inelastic effects, [New J. Phys. **15**, 013014 \(2013\)](#).
- [36] M. Saha, B. P. Venkatesh, and B. K. Agarwalla, Quantum transport in quasiperiodic lattice systems in the presence of Büttiker probes, [Phys. Rev. B **105**, 224204 \(2022\)](#).
- [37] D. Roy and G. S. Agarwal, Quantum noise induced nonreciprocity for single photon transport in parity-time symmetric systems, [arXiv:2407.00758 \(2024\)](#).
- [38] Z. Yu and S. Fan, Complete optical isolation created by indirect interband photonic transitions, [Nat. Photon. **3**, 91 \(2009\)](#).
- [39] G. S. Agarwal and K. Qu, Spontaneous generation of photons in transmission of quantum fields in PT -symmetric optical systems, [Phys. Rev. A **85**, 031802 \(2012\)](#).
- [40] J. M. P. Nair, M. O. Scully, and G. S. Agarwal, Topological transitions in dissipatively coupled Su-Schrieffer-Heeger models, [Phys. Rev. B **108**, 184304 \(2023\)](#).
- [41] B. Min, K. Agarwal, and D. Segal, Role of bath-induced many-body interactions in the dissipative phases of the Su-Schrieffer-Heeger model, [arXiv:2406.13878 \(2024\)](#).

Supplementary Material for “Nonreciprocal electrical transport in linear systems with balanced gain and loss in the bulk”

Rupak Bag and Dibyendu Roy

Raman Research Institute, Bangalore 560080, India

I. MASTER EQUATION APPROACH FOR CHARGE TRANSPORT IN A 1-D LATTICE

In this section, we give details of the master equation approach described in the main article to study charge transport in a 1-D lattice coupled to $N_i/2 = N/2 - 1$ pairs of sources (S's) and drains (D's). The length of the lattice is denoted by $L = (N - 1)a$. Using Eqs. (1-5) in the main text, we write the following steady-state equations for the density fields of the right- and left-moving particles:

$$\rho^+(a) = \rho^+(0), \quad \rho^-(a) = p\rho^-(2a), \quad (1)$$

$$[p - (p - 1)\delta_{x,2a}]\rho^+(x - a) - p\rho^+(x) + (1 - p)[\rho^-(x) - \rho^+(x)] + (-1)^{\frac{x}{a}} \frac{I_g}{2ev_F} = 0, \quad (2)$$

$$[p - (p - 1)\delta_{x,(N-1)a}]\rho^-(x + a) - p\rho^-(x) + (1 - p)[\rho^+(x) - \rho^-(x)] + (-1)^{\frac{x}{a}} \frac{I_g}{2ev_F} = 0, \quad (3)$$

$$p\rho^+(L) = \rho^+(L + a), \quad \rho^-(L + a) = \rho^-(L + 2a), \quad (4)$$

where $x \in [2a, L]$, and we denote $v_F = a/\tau$ as the group velocity of the mobile charges. The boundary conditions for the above equations are mentioned in the main article.

A. Boundary and bulk currents

Here, we derive various current formulae using the continuity equations for the charge densities. The total charge density, at any location x (and time t) is $e[\rho^+(x, t) + \rho^-(x, t)]$. We first focus on the left boundary of the lattice. Utilizing the master equations in the main article, we get:

$$e \frac{\partial}{\partial t} [\rho^+(a, t) + \rho^-(a, t)] = ev_F \left[\frac{\rho^+(0, t) - \rho^-(a, t)}{a} \right] - ev_F \left[\frac{\rho^+(a, t) - p\rho^-(2a, t)}{a} \right], \quad (5)$$

where, we use $\frac{\partial \rho^\pm(x, t)}{\partial t} \equiv [\rho^\pm(x, t + \tau) - \rho^\pm(x, t)]/\tau$. Now, we can identify the charge current flowing into the lattice as follows: $I_{\text{in}} = ev_F[\rho^+(a, t) - p\rho^-(2a, t)]$. Similarly, at the right boundary, we get :

$$e \frac{\partial}{\partial t} [\rho^+(L + a, t) + \rho^-(L + a, t)] = ev_F \left[\frac{p\rho^+(L, t) - \rho^-(L + a, t)}{a} \right] - ev_F \left[\frac{\rho^+(L + a, t) - \rho^-(L + 2a, t)}{a} \right]. \quad (6)$$

Moreover, the charge current flowing out of the lattice is defined using $I_{\text{out}} := ev_F[p\rho^+(L, t) - \rho^-(L + a, t)]$. Next, we obtain the continuity equation for the other sites $x \in \{3a, 4a, \dots, L - a\}$ in the bulk:

$$e \frac{\partial}{\partial t} [\rho^+(x, t) + \rho^-(x, t)] = epv_F \frac{\rho^+(x - a, t) - \rho^-(x, t)}{a} - epv_F \frac{\rho^+(x, t) - \rho^-(x + a, t)}{a} + (-1)^{\frac{x}{a}} \frac{I_g}{a}. \quad (7)$$

This gives the current flowing inside the lattice from site x to $x + a$ as $J(x) := epv_F[\rho^+(x, t) - \rho^-(x + a, t)]$. For odd (even) sites x , $J(x)$ gives the inter-(intra-) bond current within the lattice.

B. Single S-D dimer

Let us first consider the case of a single pair ($N_i/2 = 1$) of S and D coupled at sites $x = 2a$ and $x = 3a$, respectively. The linear set of equations in Eqs. (1-4) can be inverted easily, and we obtain the following solutions ($p \neq 0$) for the density fields in the steady state:

$$\rho^-(a) = \frac{2(1 - p)[\frac{I_g}{2ev_F} + \delta\rho]}{3 - 2p} + \rho_o, \quad (8)$$

$$\rho^+(2a) = \frac{(2 - p)[\frac{I_g}{2ev_F} + \delta\rho] + (3 - 2p)\rho_o}{p(3 - 2p)}, \quad (9)$$

$$\rho^-(2a) = \frac{\rho_o + 2(1 - p)[\frac{I_g}{2ev_F} + \delta\rho + \rho_o]}{p(3 - 2p)}, \quad (10)$$

$$\rho^+(3a) = \frac{(p - 1)\frac{I_g}{ev_F} + \delta\rho + (3 - 2p)\rho_o}{p(3 - 2p)}, \quad (11)$$

$$\rho^-(3a) = \frac{(p - 2)\frac{I_g}{2ev_F} + (1 - p)\delta\rho + (3 - 2p)\rho_o}{p(3 - 2p)}, \quad (12)$$

$$\rho^+(4a) = \frac{(p - 1)\frac{I_g}{ev_F} + \delta\rho + (3 - 2p)\rho_o}{3 - 2p}. \quad (13)$$

Therefore, the current flowing in (out of) the lattice is

$$I_{\text{in}} = I_{\text{out}} = \frac{ev_F \delta\rho - (1 - p)I_g}{3 - 2p}, \quad (14)$$

and the current between the S-D bond is

$$J(2a) = \frac{ev_F \delta\rho + (2 - p)I_g}{3 - 2p}. \quad (15)$$

The above solutions suggest that the density field at the middle sites diverges as $1/p$ if we take $p \rightarrow 0$ (large inter-conversion). On the other hand, the middle current $J(2a)$ in the limit $p \rightarrow 0$ remains finite, since $J(2a) \propto p[\rho^+(2a) - \rho^-(3a)]$.

C. Multiple S-D dimers in a long lattice

Next, we follow an iterative procedure to find the density profile in an extended lattice ($N > 4$). At the odd sites $x = 3a, 5a, \dots, (N-1)a$ in the middle of the lattice, we get:

$$\rho^-(x) = \frac{\rho_0 + [(N-2)\rho_0 + N\delta\rho - \frac{x}{a}(\delta\rho + \frac{I_g}{2ev_F})](1-p) - (2p-1)\frac{I_g}{2ev_F}}{p[1+(N-2)(1-p)]}, \quad (16)$$

$$\rho^+(x) = \frac{\rho_0 + [(N-2)\rho_0 + N\delta\rho - \frac{x}{a}(\delta\rho + \frac{I_g}{2ev_F})](1-p) + p\delta\rho + (1-p)\frac{I_g}{2ev_F}}{p[1+(N-2)(1-p)]}. \quad (17)$$

Similarly, at the even sites $x = 2a, 4a, \dots, (N-2)a$, we get :

$$\rho^-(x) = \frac{\rho_0 + [(N-2)\rho_0 + N\delta\rho - \frac{x}{a}(\delta\rho + \frac{I_g}{2ev_F})](1-p) + N(1-p)\frac{I_g}{2ev_F}}{p[1+(N-2)(1-p)]}, \quad (18)$$

$$\rho^+(x) = \frac{\rho_0 + [(N-2)\rho_0 + N\delta\rho - \frac{x}{a}(\delta\rho + \frac{I_g}{2ev_F})](1-p) + p\delta\rho + [N - (N-1)p]\frac{I_g}{2ev_F}}{p[1+(N-2)(1-p)]}. \quad (19)$$

The above expressions exclude solutions at the boundaries of the lattice, and they are given by

$$\rho^-(a) = \frac{(N-2)(1-p)[\delta\rho + \frac{I_g}{2ev_F}]}{1+(N-2)(1-p)} + \rho_0, \quad (20)$$

$$\rho^+(L+a) = \frac{(\rho_0 + \delta\rho) + (N-2)(1-p)[\rho_0 - \frac{I_g}{2ev_F}]}{1+(N-2)(1-p)}. \quad (21)$$

Utilizing the above density fields, we obtain the intra-bond currents in the lattice as follows :

$$J(x) = \frac{ev_F\delta\rho + I_g/2}{1+(N-2)(1-p)} + \frac{I_g}{2}, \quad (22)$$

where $x = 2a, 4a, \dots, (N-2)a$. The inter-bond currents in the lattice are obtained as $J(x) = \frac{ev_F\delta\rho - (1-p)(N/2-1)I_g}{1+(N-2)(1-p)} = I_{in} = I_{out}$, where $x = 3a, 5a, \dots, (N-3)a$, which are the currents in Eq. (7) of the main text.

D. Multiple S-D dimers in the continuous limit

Next, we will consider the continuum limit ($a \rightarrow 0$) of the extended lattice model with multiple S-D dimers. We take a large number of dimers ($N_i/2 \gg 1$) and use a bipartite lattice description to make further progress. We introduce $X_e = 2ma$

for $m = 1, \dots, N/2$, and $X_o = (2m-1)a$ for $m = 1, \dots, N/2$ to denote the positions of even and odd sites, respectively. Our goal is to rewrite Eqs. (1-4) with the help of the redefined coordinates, X_e and X_o . Then, we decouple the equations for the density fields on the even sublattice from those on the odd sublattice. The resulting recurrence equations will no longer contain the inhomogeneous driving term I_g , and we can take the continuum limit $a \rightarrow 0$ (along with $\tau \rightarrow 0$) to describe the density field of the particles on separate sublattices.

To facilitate such a treatment, we will consider the limit $p \rightarrow 1$ on all the hopping probabilities, but retain a finite conversion rate $\lim[(1-p)/\tau] \neq 0$ at all the middle sites of the lattice where the S and D are coupled. With these assumptions, the steady-state equations at the middle sites become:

$$\rho^\pm(X_e \mp a) = \rho^\pm(X_e) \pm \frac{a}{l_c} [\rho^+(X_e) - \rho^-(X_e)] - \frac{I_g}{2ev_F}, \quad (23)$$

$$\rho^\pm(X_o \mp a) = \rho^\pm(X_o) \pm \frac{a}{l_c} [\rho^+(X_o) - \rho^-(X_o)] + \frac{I_g}{2ev_F}, \quad (24)$$

where $X_e \in \{2a, 4a, \dots, L-a\}$, and $X_o \in \{3a, 5a, \dots, L\}$. Here, $l_c = a/(1-p)$ denotes the scattering length scale in the problem.

Equation for $\rho^+(X_o)$: Utilizing the above equations on the even sublattice, we get:

$$\rho^+(X_e) - \rho^-(X_e) = \frac{\rho^+(X_e - a) - \rho^-(X_e + a)}{1 + 2(a/l_c)}, \quad (25)$$

where $X_e = 2a, 4a, \dots, L-a$. We focus on the steady-state equations for the right-moving charges at the odd sites. If X_o is an odd site, then $(X_o - a)$ will be positioned on the even sublattice. With the help of Eq. (25), the equations at even sites $X_e = X_o - a$ for the right-moving particles become:

$$\rho^+(X_o - a) = \rho^+(X_o - 2a) - \frac{a}{2a + l_c} [\rho^+(X_o - 2a) - \rho^-(X_o)] + \frac{I_g}{2ev_F}, \text{ for } X_o = 3a, 5a, \dots, L. \quad (26)$$

By substituting the above expression for $\rho^+(X_o - a)$ into Eq. (24), the inhomogeneous term $I_g/(2ev_F)$ cancels out and we arrive at the relations:

$$\rho^+(X_o - \delta X_o) - \rho^+(X_o) - \frac{a[\rho^+(X_o - \delta X_o) - \rho^-(X_o)]}{2a + l_c} - \frac{a}{l_c} [\rho^+(X_o) - \rho^-(X_o)] = 0, \quad X_o = 3a, 5a, \dots, L. \quad (27)$$

In the above recurrence equations, the density fields on the odd sublattice are decoupled from those on the even sublattice. Here, $\delta X_o = 2a$ represents the lattice constant of the odd sublattice. We divide both sides of Eqs. (27) by δX_o and assume the continuum limit $a \rightarrow 0$. This leads to the following first-order differential equation:

$$\frac{\partial \rho^+(X_o)}{\partial X_o} + \frac{1}{l_c} [\rho^+(X_o) - \rho^-(X_o)] = 0. \quad (28)$$

The variable X_e now assumes continuous values within the interval $(0, L]$, and the boundary condition for the equation is fixed by $\rho^+(X_o = 0^+) = \rho_o + \delta\rho$. Next, we derive a similar equation for the left-moving particles.

Equation for $\rho^-(X_o)$: Following the method of the previous paragraph, we now use $X_e = X_o + a$ and rewrite Eq. (23) for the left-moving particles as follows :

$$\rho^-(X_o + a) = \rho^-(X_o + 2a) + \frac{a}{2a + l_c} [\rho^+(X_o) - \rho^-(X_o + 2a)] + \frac{I_g}{2ev_F}, \text{ for } X_o = a, 3a, \dots, L - 2a. \quad (29)$$

Substituting this expression into Eq.(24) gives the following decoupled equations :

$$\rho^-(X_o + \delta X_o) - \rho^-(X_o) + \frac{a[\rho^+(X_o) - \rho^-(X_o + \delta X_o)]}{2a + l_c} + \frac{a}{l_c} [\rho^+(X_o) - \rho^-(X_o)] = 0, \quad X_o = 3a, \dots, L - 2a. \quad (30)$$

The boundary value for the above recurrence relations is fixed at the rightmost site on the even sublattice, i.e., $X_o = L$. Using the steady-state equation at $x = L$, we get

$$\begin{aligned} \rho^-(L) &= \rho^-(L + a) - \frac{I_g}{2ev_F} + (1 - p)\rho^+(L) \\ &= \rho_o - \frac{I_g}{2ev_F} + a \left[\frac{\rho^+(L)}{l_c} \right] \\ &= \rho_o - \frac{I_g}{2ev_F} + \mathcal{O}(a), \end{aligned} \quad (31)$$

where the last term in the above expression is of the order of a . We divide both sides of Eqs. (30) by δX_o and take the limit $a \rightarrow 0$. This yields :

$$\frac{\partial \rho^-(X_o)}{\partial X_o} + \frac{1}{l_c} [\rho^+(X_o) - \rho^-(X_o)] = 0. \quad (32)$$

Once again, X_o in the above equation is a continuous parameter within the interval $(0, L]$ and the boundary value for Eq. (32) becomes $\rho^-(X_o = L) \approx \rho_o - I_g/(2ev_F)$, after neglecting all the terms in $\rho^-(X_o = L)$ that are of the order of a .

Equation for $\rho^\pm(X_e)$: One can check that the recurrence equations for the density field of the right-moving particles at even sites take the same form as Eqs. (27), where X_o is replaced by $X_e = 4a, 6a, \dots, L - a$ and δX_o is replaced by $\delta X_e = 2a$. Here, the boundary value is fixed at the left-most site of the even sublattice, i.e., $X_e = 2a$, which is given by the following relation

$$\begin{aligned} \rho^+(2a) &= \rho^+(a) + \frac{I_g}{2ev_F} + (1 - p)\rho^-(2a) \\ &= \rho_o + \delta\rho + \frac{I_g}{2ev_F} + \mathcal{O}(a). \end{aligned} \quad (33)$$

In a similar fashion, we find that $\rho^-(X_e)$ at odd sites satisfy Eqs. (30), where we replace X_o by $X_e = 2a, 4a, \dots, L - a$. At

the boundary $X_e = L + a$, we have $\rho^-(X_e = L + a) = \rho_o$. Now, X_e takes continuous values in the limit $a \rightarrow 0$ and we get:

$$\frac{\partial \rho^+(X_e)}{\partial X_e} + \frac{1}{l_c} [\rho^+(X_e) - \rho^-(X_e)] = 0, \quad X_e \in (0, L), \quad (34)$$

$$\frac{\partial \rho^-(X_e)}{\partial X_e} + \frac{1}{l_c} [\rho^+(X_e) - \rho^-(X_e)] = 0, \quad X_e \in (0, L), \quad (35)$$

where the boundary conditions for the above equations are $\rho^+(X_e = 0^+) \approx \rho_o + \delta\rho + I_g/(2ev_F)$ (after removing all terms of $\mathcal{O}(a)$ from this expression), and $\rho^-(X_e = L + 0^+) = \rho_o$, respectively.

The steady-state density solutions for the middle sites in the lattice are as follows :

$$\rho^+(X_o) = -\frac{C}{l_c} X_o + \delta\rho + \rho_o, \quad (36)$$

$$\rho^-(X_o) = \frac{C}{l_c} (L - X_o) + \rho_o - \frac{I_g}{2ev_F}, \quad (37)$$

$$\rho^+(X_e) = -\frac{C}{l_c} X_e + \delta\rho + \rho_o + \frac{I_g}{2ev_F}, \quad (38)$$

$$\rho^-(X_e) = \frac{C}{l_c} (L - X_e) + \rho_o, \quad (39)$$

where $C = [\delta\rho + I_g/(2ev_F)]/(1 + L/l_c)$. Now, the density fields at the boundaries are obtained using the relations:

$$\rho^-(X_o = a) = \lim_{\substack{p \rightarrow 1 \\ a \rightarrow 0}} p \rho^-(X_e = 2a) = \rho_o + C \frac{L}{l_c}, \quad (40)$$

$$\rho^+(X_e = L + a) = \lim_{\substack{p \rightarrow 1 \\ a \rightarrow 0}} p \rho^+(X_o = L) = \delta\rho + \rho_o - C \frac{L}{l_c}. \quad (41)$$

We observe that $\lim_{a \rightarrow 0} [\rho^-(X_o = a) - \rho^-(X_o = 3a)] = I_g/(2ev_F)$, and $\lim_{a \rightarrow 0} [\rho^+(X_e = L - a) - \rho^+(X_e = L + a)] = I_g/(2ev_F)$. Therefore, the net density field suffers a discontinuity of $I_g/(2ev_F)$ at the right (left) boundary of the even (odd) sublattice. Using the full solutions, we derive the total particle densities at the middle sites as follows:

$$\begin{aligned} \rho^+(X_e) + \rho^-(X_e) &= 2(\rho_o + \delta\rho) - \frac{2\delta\rho + I_g/(ev_F)}{l_c + L} X_e \\ &\quad - \frac{2\delta\rho - [I_g/(ev_F)](L/l_c)}{2(1 + L/l_c)} + \frac{I_g}{2ev_F}, \end{aligned} \quad (42)$$

$$\begin{aligned} \rho^+(X_o) + \rho^-(X_o) &= 2(\rho_o + \delta\rho) - \frac{2\delta\rho + I_g/(ev_F)}{l_c + L} X_o \\ &\quad - \frac{2\delta\rho - [I_g/(ev_F)](L/l_c)}{2(1 + L/l_c)} - \frac{I_g}{2ev_F}. \end{aligned} \quad (43)$$

The incoming and outgoing charge currents are

$$\begin{aligned} I_{in} &= \lim_{\substack{p \rightarrow 1 \\ a \rightarrow 0}} ev_F [\rho^+(X_o = a) - p \rho^-(X_e = 2a)] \\ &= \frac{ev_F \delta\rho}{1 + L/l_c} - \frac{I_g}{2} \left\{ 1 - \frac{1}{1 + L/l_c} \right\} = I_{out}, \end{aligned} \quad (44)$$

these are given in Eq. (8) of the main text. We use current probes for the S's and D's in the master equation treatment and in the discussion of the resistive circuit model (in the main text and Sec. IV). Next, we will discuss charge transport in the quantum regime using voltage probes for the S's and D's.

II. QUANTUM LANGEVIN EQUATION APPROACH FOR CHARGE TRANSPORT IN MICROSCOPIC MODEL

In this section, we will provide details of the microscopic analysis of charge transport through a quantum channel (wire). The wire contains N sites and is connected to microscopic baths. The full system (the wire and all the baths) is modeled by a microscopic Hamiltonian \hat{H} , given in the main article. Utilizing \hat{H} , we get the following Heisenberg equations for the operators ($\hbar = 1$):

$$\frac{\partial \hat{b}_1(l)}{\partial t} = i[\hat{b}_2(l) + \gamma_l \hat{c}_l], \quad (45)$$

$$\frac{\partial \hat{b}_m(l)}{\partial t} = i[\hat{b}_{m+1}(l) + \hat{b}_{m-1}(l)] \quad \text{for } m \neq 1, \quad (46)$$

$$\frac{\partial \hat{c}_l}{\partial t} = i(\hat{c}_{l-1} + \hat{c}_{l+1}) + i\gamma_l \hat{b}_1(l) \quad \text{for } l = 1, 2, \dots, N, \quad (47)$$

where we have taken $\gamma_0 = 1$. The open boundary condition on the wire imposes $\hat{c}_0 = \hat{c}_{N+1} = 0$. To integrate out the bath's degrees of freedom, we use the retarded Green's function operator $\hat{g}^+(l, t) = -i\theta(t)e^{-i\hat{H}_B^l t}$ for each bath located at l . The matrix elements of an operator $\hat{g}^+(l, t)$ in the real-space basis are given by

$$g_{m,n}^+(l, t) = -i\theta(t) \int_0^\pi dk \psi_k(m) \psi_k^*(n) e^{-i\omega_k t}. \quad (48)$$

Here, the energy-momentum dispersion $\omega_k = -2\cos k$ represents the single particle spectrum of \hat{H}_B^l . The corresponding wavefunctions $\psi_k(m)$ in a semi-infinite TB chain are given by $\psi_k(m) = \sqrt{2/\pi} \sin km$, where $k \in (0, \pi)$. These wavefunctions are used to define normal mode operators for the l th bath: $\hat{b}_k^\dagger(l) = \sum_m \psi_k(m) \hat{b}_m^\dagger(l)$, which diagonalizes \hat{H}_B^l . Further, $\psi_k(m)$ satisfies the following two relations: $\sum_{m \geq 1} \psi_k(m) \psi_{k'}^*(m) = \delta(k - k')$, and $\int_0^\pi dk \psi_k(m) \psi_k^*(n) = \delta_{mn}$. It is then easy to check that $\{\hat{b}_m(l), \hat{b}_{n'}^\dagger(l')\} = \delta_{mn} \delta_{ll'}$ gives $\{\hat{b}_k(l), \hat{b}_{k'}^\dagger(l')\} = \delta(k - k') \delta_{ll'}$. Using Eqs. (45-46), we obtain the following equation of motion for $\hat{b}_k(l)$:

$$\frac{\partial \hat{b}_k(l)}{\partial t} = -i\omega_k \hat{b}_k(l) + i\gamma_l \psi_k^*(1) \hat{c}_l. \quad (49)$$

Integrating the above equation from an initial time t_0 to a later time t , we get,

$$\begin{aligned} \hat{b}_k(l, t) &= \hat{b}_k(l, t_0) e^{i\omega_k(t-t_0)} + i\gamma_l \psi_k^*(1) \int_{t_0}^t d\tau \hat{c}_l(\tau) e^{-i\omega_k(t-\tau)}, \\ \hat{b}_m(l, t) &= i \sum_n g_{m,n}^+(l, t-t_0) \hat{b}_n(l; t_0) \\ &\quad - \gamma_l \int_{t_0}^t d\tau g_{m,1}^+(l, t-\tau) \hat{c}_l(\tau), \quad \text{where } t > t_0. \end{aligned} \quad (50)$$

In the previous line, we have used the relation $\hat{b}_m^\dagger(l, t) = \int dk \psi_k^*(m) \hat{b}_k^\dagger(l, t)$. Next, we substitute the expression for $\hat{b}_1(l, t)$ at a later time t into Eqs. (47). This will lead to the generalized quantum Langevin equations for the wire's degree of freedom :

$$\begin{aligned} \frac{\partial \hat{c}_l}{\partial t} &= i(\hat{c}_{l+1} + \hat{c}_{l-1}) - i\hat{\eta}_l(t) \\ &\quad - i \int_{t_0}^t d\tau \Sigma_l^+(t-\tau) \hat{c}_l(\tau) \quad \text{for } l = 1, 2, \dots, N. \end{aligned} \quad (51)$$

We introduce the self-energy correction, $\Sigma_l^+(t)$ in the time domain and the noise operator, $\hat{\eta}_l(t)$ as:

$$\begin{aligned} \hat{\eta}_l(t) &= -i \gamma_l \sum_m g_{1,m}^+(l, t-t_0) \hat{b}_m(l, t_0) \quad \text{and,} \\ \Sigma_l^+(t) &= \gamma_l^2 g_{1,1}^+(l, t). \end{aligned} \quad (52)$$

They both appear because of a finite coupling of the wire with a bath located at site l .

A. Steady-state equations and noise correlations

Next, we explore the charge transport through the wire in the steady state ($t \rightarrow \infty$). Let us assume that the wire was coupled to the baths in the remote past ($t_0 \rightarrow -\infty$). This simplifies the analysis by facilitating Fourier transformation in the frequency domain. The Fourier transformations from the time domain to the frequency domain for the operators and complex numbers are:

$$\begin{aligned} \hat{c}_l(\omega) &= \frac{1}{2\pi} \int_{-\infty}^{\infty} dt e^{i\omega t} \hat{c}_l(t), \quad \hat{\eta}_l(\omega) = \frac{1}{2\pi} \int_{-\infty}^{\infty} dt e^{i\omega t} \hat{\eta}_l(t), \\ \text{and } \Sigma_l^+(\omega) &= \gamma_l^2 \int_{-\infty}^{\infty} dt e^{i\omega t} g_{1,1}^+(l, t). \end{aligned} \quad (53)$$

Using the inverse Fourier transformation of the above relations, we transform the quantum Langevin equations in Eqs. (51) into

$$\hat{c}_{l-1}(\omega) + [\omega - \Sigma_l^+(\omega)] \hat{c}_l(\omega) + \hat{c}_{l+1}(\omega) = \hat{\eta}_l(\omega), \quad (54)$$

for $l = 1, 2, \dots, N$. The above equations are linear in the operators $\hat{c}_l(\omega)$ with the noises appearing as inhomogeneous terms on the right-hand side. Therefore, we can invert Eqs. (54) to get the steady-state solutions in the frequency domain as follows :

$$\hat{c}_l(\omega) = \sum_{l'=1}^N G_{ll'}^+(\omega) \hat{\eta}_{l'}(\omega) \quad \text{for } l = 1, 2, \dots, N, \quad (55)$$

where $G_{ll'}^+(\omega)$ are the elements of (\hat{Z}^{-1}) . The elements of the matrix \hat{Z} have the following form : $Z_{ll'}(\omega) = \delta_{l,l'-1} + [\omega - \Sigma_l^+(\omega)] \delta_{l,l'} + \delta_{l,l'+1}$.

Following the definition in Eqs. (52), the noise in the wire enters through the bath operators $\hat{b}_m(l, t_0)$. A bath coupled to the wire at site l was initialized in a thermal state, which

is characterized by the grand canonical ensemble with temperature T and chemical potential μ_l . Therefore, the normal mode operators $\hat{b}_k^\dagger(l), \hat{b}_k(l)$ satisfy the following average relations: $\langle \hat{b}_k^\dagger(l, t_o) \rangle = 0, \langle \hat{b}_k(l, t_o) \rangle = 0$ and $\langle \hat{b}_k^\dagger(l, t_o) \hat{b}_{k'}(l', t_o) \rangle = f_l(\omega_k) \delta(k - k') \delta_{l, l'}$. Here, $f_l(\omega)$ represents the Fermi function, expressed as $f_l(\omega) = [e^{(\omega - \mu_l)/K_B T} + 1]^{-1}$ and K_B stands for the Boltzmann constant. As a consequence of the above relations, we immediately obtain $\langle \hat{\eta}_l(t) \rangle = \langle \hat{\eta}_l^\dagger(t) \rangle = 0$. We are interested in finding the average charge currents across various bonds in the wire. This requires two-point correlations in noise operators. The noise correlations arising from a bath at site l , between any two times t and t' are given by

$$\begin{aligned} & \langle \hat{\eta}_l^\dagger(t) \hat{\eta}_l(t') \rangle \\ &= \gamma_l^2 \sum_{m,n} g_{1,m}^{+*}(l, t - t_o) g_{1,n}^+(l; t' - t_o) \langle \hat{b}_m^\dagger(l, t_o) \hat{b}_n(l, t_o) \rangle \\ &= \gamma_l^2 \sum_{m,n} g_{1,m}^{+*}(l, t - t_o) g_{1,n}^+(l; t' - t_o) \int_0^\pi dk \psi_k^*(m) \psi_k(n) f_l(\omega_k) \\ &= \gamma_l^2 \int_0^\pi dk |\psi_k(1)|^2 f_l(\omega_k) e^{-i\omega_k(t' - t)}. \end{aligned} \quad (56)$$

Thus, the noises from the baths are colored. They arise due to the finite bandwidth and nonlinear dispersion of the structured TB baths. In the frequency domain, the noise correlations get simplified to

$$\begin{aligned} \langle \hat{\eta}_l^\dagger(\omega) \hat{\eta}_l(\omega') \rangle &= \frac{1}{(2\pi)^2} \int \int dt dt' e^{-i\omega t} e^{i\omega' t'} \langle \hat{\eta}_l^\dagger(t) \hat{\eta}_l(t') \rangle \\ &= \gamma_l^2 f_l(\omega) \rho_l(\omega) \delta(\omega - \omega'), \end{aligned} \quad (57)$$

where $\rho_l(\omega_k) = |\psi_k(1)|^2 / |\partial_k \omega_k|$ gives the density of states at the first site of the l th bath. For a semi-infinite TB chain, we get $\rho_l(\omega_k) = \sqrt{4 - \omega_k^2} / (2\pi)$.

We now calculate the self-energy correction in the frequency domain resulting from connecting a bath to the wire at site l .

$$\begin{aligned} \Sigma_l^+(\omega) &= \gamma_l^2 \int_{-\infty}^{\infty} dt e^{i\omega t} g_{1,1}^+(l, t) \\ &= -i\gamma_l^2 \int_{-\infty}^{\infty} dt \theta(t) \langle 1(l) | e^{i(\omega - \hat{H}_B^l)t} | 1(l) \rangle \\ &= -i\gamma_l^2 \int_0^{\infty} dt \lim_{\varepsilon \rightarrow 0^+} \langle 1(l) | e^{i(\omega - \hat{H}_B^l + i\varepsilon)t} | 1(l) \rangle \\ &= \gamma_l^2 \lim_{\varepsilon \rightarrow 0^+} \langle 1(l) | (\omega - \hat{H}_B^l + i\varepsilon)^{-1} | 1(l) \rangle \\ &= \frac{\gamma_l^2}{2} (\omega - i\sqrt{4 - \omega^2}) = \Delta_l(\omega) - i\frac{\Gamma_l(\omega)}{2}. \end{aligned} \quad (58)$$

In the above derivation, we use $\hat{b}_m^\dagger(l)|\varphi\rangle \equiv |m(l)\rangle$, where $|\varphi\rangle$ is the vacuum mode of the coupled system (wire and the bath). In Eq. (58), we have separated the real and imaginary parts of the self-energy $\Sigma_l^+(\omega)$. The real part gives the frequency-dependent energy shift on the wire's onsite energies and is given by: $\Delta_l(\omega) = \gamma_l^2 \omega / 2$. The imaginary part is always negative, and it introduces dissipation in the wire. Using the expression for $\rho_l(\omega)$, we can rewrite $\Gamma_l(\omega) = 2\pi\gamma_l^2 \rho_l(\omega)$.

We can relate the noise correlations with the dissipative component of the self-energy through the following (fluctuation-dissipation) relation:

$$\langle \eta_l^\dagger(\omega) \eta_l(\omega') \rangle = \frac{\Gamma_l(\omega)}{2\pi} f_l(\omega) \delta(\omega - \omega'). \quad (59)$$

B. Charge currents in the steady state

We again apply a continuity equation to obtain various currents in the system. Let us define the local particle density at site l in the wire as $n_l = \langle \hat{c}_l^\dagger \hat{c}_l \rangle$. We use the equations of motion in Eqs. (45-47) to derive the time rate of change of local charge density at site l :

$$\begin{aligned} \frac{\partial \langle n_l \rangle}{\partial t} &= ie\gamma_l \langle \hat{c}_l^\dagger \hat{b}_1(l) - \hat{b}_1^\dagger(l) \hat{c}_l \rangle + ie \langle \hat{c}_l^\dagger \hat{c}_{l-1} - \hat{c}_{l-1}^\dagger \hat{c}_l \rangle \\ &\quad - ie \langle \hat{c}_{l+1}^\dagger \hat{c}_l - \hat{c}_l^\dagger \hat{c}_{l+1} \rangle. \end{aligned} \quad (60)$$

Using the above expression, we identify two kinds of charge currents in the wire:

$$J_l = ie \langle \hat{c}_{l+1}^\dagger \hat{c}_l - \hat{c}_l^\dagger \hat{c}_{l+1} \rangle, \quad (61)$$

$$I_l = ie\gamma_l \langle \hat{c}_l^\dagger \hat{b}_1(l) - \hat{b}_1^\dagger(l) \hat{c}_l \rangle = 2e\gamma_l \text{Im} \langle \hat{b}_1^\dagger(l) \hat{c}_l \rangle. \quad (62)$$

The current flowing through the wire from left to right across the bond between the sites l and $l+1$ is represented by J_l . Similarly, the current entering the wire through the junction between the first site of the l th bath and site l of the wire is denoted by I_l . In the steady state, we utilize the noise correlations in the frequency domain to derive expressions for J_l and I_l . From Eq. (61), we get:

$$\begin{aligned} J_l &= ie \int \int d\omega d\omega' e^{i(\omega - \omega')t} \langle \hat{c}_{l+1}^\dagger(\omega) \hat{c}_l(\omega') - \hat{c}_l^\dagger(\omega) \hat{c}_{l+1}(\omega') \rangle \\ &= ie \int d\omega \sum_{l'} [G_{l'l+1}^-(\omega) G_{ll'}^+(\omega) - G_{l'l}^-(\omega) G_{l+1l'}^+(\omega)] \\ &\quad \times \gamma_{l'}^2 \rho_{l'}(\omega) f_{l'}(\omega) \\ &= \frac{e}{2\pi} \int d\omega \sum_{l'} \mathcal{F}_{ll'}(\omega) [f_l(\omega) - f_{l'}(\omega)]. \end{aligned} \quad (63)$$

In the above equation, we introduce $G_{ll'}^-(\omega) \equiv G_{ll'}^{+*}(\omega)$ and $\mathcal{F}_{ll'}(\omega) = i[G_{ll'}^-(\omega) G_{l+1l'}^+(\omega) - G_{l'l+1}^-(\omega) G_{ll'}^+(\omega)] \Gamma_{l'}(\omega)$. We also use $\sum_{l'} \mathcal{F}_{ll'}(\omega) = 0$, which can be demonstrated using the following two relations:

$$i \sum_{l=1}^N G_{il}^+(\omega) \Gamma_l(\omega) G_{lj}^-(\omega) = G_{ij}^-(\omega) - G_{ij}^+(\omega), \quad (64)$$

$$\text{Re}[G_{ll'}^+(\omega)] = \text{Re}[G_{l'l}^-(\omega)]. \quad (65)$$

We then simplify the expression for the current I_l in Eq. (62) that flows in the wire from a bath located at site l .

$$\begin{aligned} I_l &= -2e \text{Im} \left[\int \int d\omega d\omega' e^{i(\omega - \omega')t} \left\langle \{ \hat{\eta}_l^\dagger(\omega) \right. \right. \\ &\quad \left. \left. + \Sigma_l^{+*}(\omega) \hat{c}_l^\dagger(\omega) \} \hat{c}_l(\omega') \right\rangle \right] \end{aligned}$$

$$\begin{aligned}
&= -2e\text{Im} \left[\int \int d\omega d\omega' e^{i(\omega-\omega')t} \left\{ \sum_j G_{lj}^+(\omega) \langle \hat{\eta}_l^\dagger(\omega) \hat{\eta}_j(\omega') \rangle \right. \right. \\
&\quad \left. \left. + \Sigma_l^{+*}(\omega) \sum_{i,j} G_{li}^{+*}(\omega) G_{lj}^+(\omega') \langle \hat{\eta}_i^\dagger(\omega) \hat{\eta}_j(\omega') \rangle \right\} \right] \\
&= -2e \int d\omega \left\{ \text{Im} [G_{ll}^+(\omega)] \gamma_l^2 \rho_l(\omega) f_l(\omega) \right. \\
&\quad \left. + \text{Im} [\Sigma_l^{+*}(\omega)] \sum_{l'} |G_{ll'}^+(\omega)|^2 \gamma_{l'}^2 \rho_{l'}(\omega) f_{l'}(\omega) \right\} \\
&= -\frac{e}{2\pi} \int d\omega \left\{ -\sum_{l'} G_{ll'}^+(\omega) \Gamma_{l'}(\omega) G_{l'l}^-(\omega) f_l(\omega) \Gamma_l(\omega) \right. \\
&\quad \left. + \Gamma_l(\omega) \sum_{l'} |G_{ll'}^+(\omega)|^2 f_{l'}(\omega) \Gamma_{l'}(\omega) \right\} \\
&= \frac{e}{2\pi} \sum_{l'} \int d\omega \mathcal{T}_{ll'}(\omega) [f_l(\omega) - f_{l'}(\omega)]. \quad (66)
\end{aligned}$$

Here, we define the transmission coefficients between two baths located at sites l and l' by $\mathcal{T}_{ll'}(\omega) = |G_{ll'}^+(\omega)|^2 \Gamma_l(\omega) \Gamma_{l'}(\omega)$.

The current formulae in Eq. (63) and Eq. (66) are expressed as integrals over all frequencies in the Fourier domain. For analytical purposes, we can further simplify these expressions. We give a detailed derivation for I_l expanded in all powers of $\delta\mu_l = \mu_l - \bar{\mu}$. Let us introduce the integration variable $z = \beta(\omega - \bar{\mu})$, where β is reciprocal of the temperature T , i.e., $\beta = (K_B T)^{-1}$. We perform a Taylor series expansion of $f_l(\omega)$ about $\mu_l = \bar{\mu}$. Then, the differences in the Fermi functions can be written as follows:

$$\begin{aligned}
f_l(\omega) - f_{l'}(\omega) &= \sum_{n \geq 1} \frac{1}{n!} \frac{\partial^n f_l(\omega)}{\partial \omega^n} \Big|_{\mu_l = \bar{\mu}} (\delta\mu_l^n - \delta\mu_{l'}^n) \\
&= \sum_{n \geq 1} \frac{(-1)^n \beta^n}{n!} \frac{\partial^n}{\partial z^n} (1 + e^z)^{-1} (\delta\mu_l^n - \delta\mu_{l'}^n). \quad (67)
\end{aligned}$$

Similarly, we carry out a series expansion for the transmission coefficients $\mathcal{T}_{ll'}(\omega)$ about $\omega = \bar{\mu}$ and write Eq. (66) as:

$$\begin{aligned}
I_l &= \frac{e}{2\pi} \sum_{l'=1}^N \sum_{n \geq 1} \sum_{m=0}^{\infty} \frac{(-1)^n}{n! m!} \beta^{n-(m+1)} \mathcal{T}_{ll',m} \\
&\quad \times (\delta\mu_l^n - \delta\mu_{l'}^n) \int_{-\infty}^{\infty} dz z^m \frac{\partial^n}{\partial z^n} (1 + e^z)^{-1}. \quad (68)
\end{aligned}$$

Here, we use the notation $\mathcal{T}_{ll',m} = \frac{\partial^m}{\partial \omega^m} \mathcal{T}_{ll'}(\omega) \Big|_{\omega = \bar{\mu}}$. At temperatures $T \ll \bar{\mu}/K_B$, the terms in the series containing $\beta^{n-(m+1)}$ for $n < m+1$ can be neglected. Now, for $n \geq m+1$, the above integration (by repetitive integrations by-parts) gives:

$$\int_{-\infty}^{\infty} dz z^m \frac{\partial^n}{\partial z^n} (1 + e^z)^{-1} = \delta_{m,n-1} (-1)^n (n-1)!, \quad (69)$$

where $n!$ denotes the factorial value of an integer n . Therefore, at temperatures $T \ll \bar{\mu}/K_B$, the current I_l due to the applied chemical potential biases $\delta\mu_l$ can be written as

$$I_l \approx \frac{e}{2\pi} \sum_{l'=1}^N \sum_{n \geq 1} \frac{1}{n!} \mathcal{T}_{ll',n-1} (\delta\mu_l^n - \delta\mu_{l'}^n). \quad (70)$$

Similarly, we can get

$$J_l \approx \frac{e}{2\pi} \sum_{l'=1}^N \sum_{n \geq 1} \frac{1}{n!} \mathcal{F}_{ll',n-1} (\delta\mu_l^n - \delta\mu_{l'}^n), \quad (71)$$

where $\mathcal{F}_{ll',m} = \frac{\partial^m}{\partial \omega^m} \mathcal{F}_{ll'}(\omega) \Big|_{\omega = \bar{\mu}}$. We have used $\mathcal{T}_{ll',0} \equiv \mathcal{T}_{ll'}$, and $\mathcal{F}_{ll',0} \equiv \mathcal{F}_{ll'}$ in the main article. In the linear response regime, we truncate the series in Eqs. (70,71) after $n = 1$.

C. One S-D dimer: linear and nonlinear response regime

We consider a single S-D dimer ($N_i/2 = 1$). The transmission coefficients $\mathcal{T}_{ll'}$ are symmetric in l and j , and we derive them fully analytically as follows:

$$\mathcal{T}_{24} = \mathcal{T}_{31} = \frac{4\gamma^2}{\mathcal{D}(\bar{\mu})} (1 - \bar{\mu}^2/4), \quad (72)$$

$$\mathcal{T}_{23} = \frac{4\gamma^4}{\mathcal{D}(\bar{\mu})} (1 - \bar{\mu}^2/4), \quad \mathcal{T}_{14} = \frac{4}{\mathcal{D}(\bar{\mu})} (1 - \bar{\mu}^2/4), \quad (73)$$

$$\mathcal{T}_{21} = \mathcal{T}_{34} = \frac{4\gamma^2}{\mathcal{D}(\bar{\mu})} (1 - \bar{\mu}^2/4) [1 + \gamma^4 - \gamma^2(\bar{\mu}^2 - 2)], \quad (74)$$

where $\mathcal{D}(\bar{\mu}) = (2 + 2\gamma^2 + \gamma^4)^2 - (1 + 2\gamma^2 + 5\gamma^4 + 2\gamma^6)\bar{\mu}^2 + \gamma^4\bar{\mu}^4$. Using the S and D current constraints, i.e., $I_l = (-1)^l I_g$ for $l = 2, 3$, we obtain: $\mu_2 = \bar{\mu} + \Delta_\mu$ and $\mu_3 = \bar{\mu} - \Delta_\mu$ in the linear response regime. Here

$$\Delta_\mu = \frac{2\pi(I_g/e) + (\mathcal{T}_{34} - \mathcal{T}_{13})(\mu_L - \bar{\mu})}{\mathcal{T}_{13} + \mathcal{T}_{34} + 2\mathcal{T}_{23}}. \quad (75)$$

The above expression gives us Eq. (13) in the main article once we make the substitution for the transmission coefficients. The current flowing in the wire from the left end is $I_1 = G_4(\delta\mu/e) - \delta I$, where

$$\begin{aligned}
G_4 &= \frac{2\mathcal{T}_{34}\mathcal{T}_{13} + 2\mathcal{T}_{23}\mathcal{T}_{14} + (\mathcal{T}_{23} + \mathcal{T}_{14})(\mathcal{T}_{34} + \mathcal{T}_{13})}{2\pi(\mathcal{T}_{13} + \mathcal{T}_{34} + 2\mathcal{T}_{23})} \\
&= e^2 \frac{(4 - \bar{\mu}^2)(2 + \gamma^4 + 2\gamma^2 - \gamma^2\bar{\mu}^2)(\gamma^2 + 1)^2}{2\pi\mathcal{D}(\bar{\mu})(2 + \gamma^4 + 4\gamma^2 - \gamma^2\bar{\mu}^2)}, \quad (76)
\end{aligned}$$

$$\delta I = \frac{(\mathcal{T}_{12} - \mathcal{T}_{13})I_g}{(\mathcal{T}_{13} + \mathcal{T}_{34} + 2\mathcal{T}_{23})} = \frac{(\gamma^4 + 2\gamma^2 - \gamma^2\bar{\mu}^2)}{(2 + \gamma^4 + 4\gamma^2 - \gamma^2\bar{\mu}^2)} I_g. \quad (77)$$

Equating $\delta I = I_g/3$, we get only one real solution for γ , which is given by

$$\gamma_c^2 = \frac{\bar{\mu}^2 - 1 + \sqrt{(\bar{\mu}^2 - 1)^2 + 4}}{2}, \quad (78)$$

e.g., for $\bar{\mu} = 1$, we get $\gamma_c = 1$, which is in the non-perturbative regime of the wire-bath coupling. Next, we consider the nonlinear current response. In the series expansion of I_l in Eq. (70), we will retain terms up to the third order ($n = 3$) in $\delta\mu_l$. This gives the following pair of nonlinear S-D equations

with $\delta\mu_2$ and $\delta\mu_3$ as the unknown variables:

$$\begin{aligned} \frac{v''}{6}\delta\mu_2^3 - \frac{w''}{6}\delta\mu_3^3 + \frac{v'}{2}\delta\mu_2^2 - \frac{w'}{2}\delta\mu_3^2 + v\delta\mu_2 - w\delta\mu_3 &= \xi_2, \\ \frac{v''}{6}\delta\mu_3^3 - \frac{w''}{6}\delta\mu_2^3 + \frac{v'}{2}\delta\mu_3^2 - \frac{w'}{2}\delta\mu_2^2 + v\delta\mu_3 - w\delta\mu_2 &= \xi_3, \end{aligned} \quad (79)$$

$$\begin{aligned} \xi_i &= (-1)^i \frac{2\pi I_g}{e} + \frac{\delta\mu}{2}(\mathcal{T}_{i1} - \mathcal{T}_{i4}) + \frac{\delta\mu^2}{8}(\mathcal{T}_{i1,1} + \mathcal{T}_{i4,1}) \\ &\quad + \frac{\delta\mu^3}{48}(\mathcal{T}_{i1,2} - \mathcal{T}_{i4,2}), \end{aligned} \quad (80)$$

where $v \equiv v(\bar{\mu}) = (\mathcal{T}_{31} + \mathcal{T}_{32} + \mathcal{T}_{34})$, $w \equiv w(\bar{\mu}) = \mathcal{T}_{32}$; $v' = \partial_{\bar{\mu}} v$, $v'' = \frac{\partial^2 v}{\partial \bar{\mu}^2}$ and similarly for w . Due to the coupled nonlinearity for $\delta\mu_2$ and $\delta\mu_3$ in Eqs. (79), we can get many pairs of complex solutions. Out of these, only one real pair $(\mu_2^{(3)}, \mu_3^{(3)})$ is of physical relevance which coincides with the linear response results in Eq. (75) for $\delta\mu_2^{(3)}, \delta\mu_3^{(3)} \leq \delta\mu$ (Fig. 1). We use this physical pair to compute the magnitude of the incoming and outgoing current $|I_l|$ in the forward and reverse bias. The main article shows the corresponding relative non-reciprocity in Fig. 1(c).

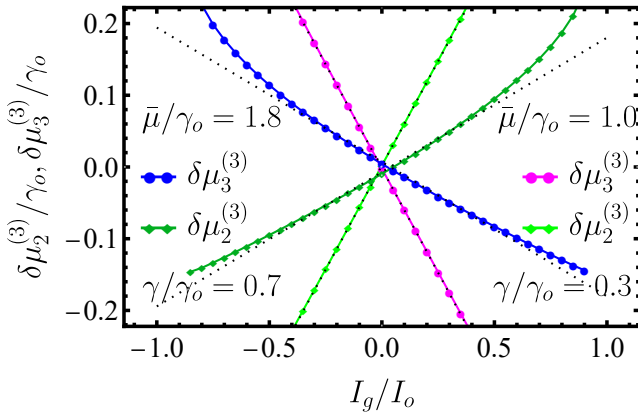


FIG. 1: Numerical roots $(\mu_2^{(3)}, \mu_3^{(3)})$ of the nonlinear Eqs. (79). The dotted black lines show the corresponding solutions obtained within the linear response analysis. In the plot, we fix $\delta\mu/\gamma_0 = 0.1$ and $e = 1$.

D. Linear response regime for the multiple dimers

Next, we focus on the multiple S-D baths in a longer quantum wire ($N \gg 4$). We restrict our calculations to the linear response regime for analytical traceability and consider a large number of S-D dimers with $N_i = N - 2$. Let us further assume $\gamma < 1$, which gives $l_c > 1$. The following parameters σ, l_c, α_R , etc., are introduced in the main text. We will show the following chemical potentials (Fig. 2) of the middle baths fix the source and drain currents self-consistently at the bulk sites,

which are located far away from the boundaries:

$$\mu_l = \mu_L - \phi + \left[\frac{l_c}{2\sigma} + (-1)^l \nabla \right] \frac{eI_g}{2} - \frac{2\phi}{l_c}(l-2), \quad (81)$$

$$\phi = \frac{\delta\mu + eI_g l_c / (2\sigma)}{2[1 + (N-3)/l_c]}, \quad \text{and} \quad \nabla = \frac{\text{coth}^2 \alpha_R}{2\sigma}, \quad (82)$$

for $l = 2, 3, \dots, N-1$. First, we compute I_l at an odd site l in the bulk, such that $1 \ll l \ll N$. Within the linear response regime, we get

$$\begin{aligned} I_l &= \frac{e}{2\pi} \sum_{l' \neq 1, N} \mathcal{F}_{ll'}(\delta\mu_l - \delta\mu_{l'}) + \frac{e}{2\pi} \mathcal{F}_{l1}(\delta\mu_l - \delta\mu_L) \\ &\quad + \frac{e}{2\pi} \mathcal{F}_{lN}(\delta\mu_l - \delta\mu_R) \\ &\approx \frac{e}{2\pi} \sum_{l' \neq 1, N} \mathcal{F}_{ll'} \left[-\frac{eI_g}{2} \nabla - (-1)^{l'} \frac{eI_g}{2} \nabla - \frac{2\phi}{l_c}(l-l') \right] \\ &= -\frac{e^2 I_g}{2\pi} \nabla \sum_{l'=2,4,\dots}^{N-2} \mathcal{F}_{ll'} - \frac{2\phi}{l_c} \frac{e}{2\pi} \sum_{l' \neq 1, N} \mathcal{F}_{ll'}(l-l'). \end{aligned} \quad (83)$$

The boundary terms in the above calculations are neglected in comparison to the other terms since the corresponding transmission coefficients are negligibly small for $1 \ll l \ll N$. Again, for all the points l, l' within the bulk of the wire, we get:

$$\mathcal{F}_{ll'} = \frac{\pi^2 \gamma^A \rho_l(\bar{\mu}) \rho_{l'}(\bar{\mu})}{|\sinh \alpha|^2} e^{-2\alpha_R |l-l'|}, \quad (84)$$

in the limit $N \rightarrow \infty$. In this limit, we can ideally get:

$$\lim_{(N-1) \rightarrow \infty} \lim_{l \rightarrow \infty} \sum_{l' \neq 1, N} e^{-2\alpha_R |l-l'|} (l-l') = 0, \quad (85)$$

$$\lim_{(N-1) \rightarrow \infty} \lim_{l \rightarrow \infty} \sum_{l'=2,4,\dots}^{N-2} e^{-2\alpha_R |l-l'|} = \frac{1}{\sinh 2\alpha_R}. \quad (86)$$

Therefore, at an odd site l in the bulk of the wire, we get

$$I_l = -\frac{e^2 I_g}{2\pi} \frac{\pi^2 \gamma^A \rho_l^2(\bar{\mu})}{|\sinh \alpha|^2} \frac{\nabla}{\sinh 2\alpha_R} = -I_g. \quad (87)$$

We have used $\sigma = e^2 \sin^2 \alpha_l \text{coth} \alpha_R / (2\pi |\sinh \alpha|^2)$, and $\rho_l(\bar{\mu}) = 2 \sin \alpha_l \sinh \alpha_R / (\pi \gamma^2)$. Similarly, we can get $I_l = I_g$ for all even points l in the bulk.

Let us calculate the inter-bond current, $J_D = J_l$ (l is odd) within the wire. In the linear response regime,

$$\begin{aligned} J_D &= \frac{e}{2\pi} \sum_{l' \neq 1, N} \mathcal{F}_{ll'}(\delta\mu_l - \delta\mu_{l'}) + \frac{e}{2\pi} \mathcal{F}_{l1}(\delta\mu_l - \delta\mu_L) \\ &\quad + \frac{e}{2\pi} \mathcal{F}_{lN}(\delta\mu_l - \delta\mu_R) \\ &\approx -\frac{e^2 I_g}{2\pi} \nabla \sum_{l'=2,4,\dots}^{N-2} \mathcal{F}_{ll'} - \frac{2\phi}{l_c} \frac{e}{2\pi} \sum_{l' \neq 1, N} \mathcal{F}_{ll'}(l-l'). \end{aligned} \quad (88)$$

Now, for all points l, l' within the bulk of the wire, we can get

$$\begin{aligned} \mathcal{F}_{ll'} &= -\frac{\pi \gamma^2 \rho_l(\bar{\mu})}{|\sinh \alpha|^2} e^{-(|l+1-l'|+|l-l'|)\alpha_R} \\ &\quad \times \sin(|l+1-l'| - |l-l'|) \alpha_l, \end{aligned} \quad (89)$$

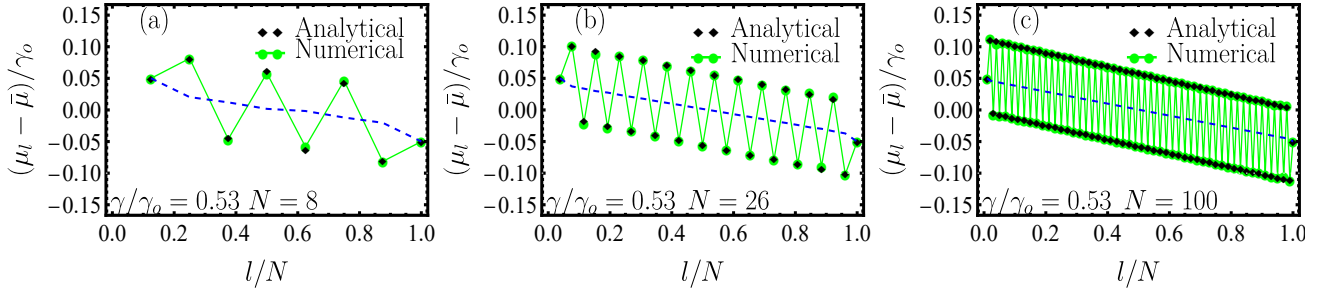


FIG. 2: Chemical potential profile in a finite quantum wire with increasing size N : (a) $N=8$, (b) $N=26$, and (c) $N=100$. We have shown an excellent agreement between the analytical and numerical plots even in smaller wires, i.e., $N \geq l_c$. The blue dashed line shows the corresponding plot for $I_g = 0$, with $\gamma \neq 0$. Here, $I_g/I_0 = 0.3$, and $\bar{\mu}/\gamma_0 = 1.0$, $\delta\mu/\gamma_0 = 0.1$, and $e = 1$.

for $N \rightarrow \infty$. Using the above relation, we evaluate the following two summations :

$$\begin{aligned} & \lim_{(N-l) \rightarrow \infty} \lim_{l \rightarrow \infty} \sum_{l' \neq 1, N} \mathcal{F}_{ll'}(l-l') \\ &= -\frac{\pi\gamma^2 \rho_l(\bar{\mu}) \cosh \alpha_R \sin \alpha_l}{|\sinh \alpha|^2 2(\sinh \alpha_R)^2} = -2\pi \frac{\sigma}{e^2}, \end{aligned} \quad (90)$$

$$\lim_{(N-l) \rightarrow \infty} \lim_{l \rightarrow \infty} \sum_{l'=2,4,\dots}^{N-2} \mathcal{F}_{ll'} = \frac{\pi\gamma^2 \rho_l(\bar{\mu}) \sin \alpha_l}{|\sinh \alpha|^2 2 \cosh \alpha_R}. \quad (91)$$

Substituting the above expressions into Eq. (88), we obtain an expression for J_D as follows:

$$\begin{aligned} J_D &= -\frac{e^2 I_g}{2\pi} \nabla \frac{\pi\gamma^2 \rho_l(\bar{\mu}) \sin \alpha_l}{|\sinh \alpha|^2 2 \cosh \alpha_R} + \frac{2\phi\sigma}{el_c} \\ &= -\frac{I_g}{2} + \frac{\sigma(\delta\mu/e) + I_g l_c/2}{l_c + (N-3)}. \end{aligned} \quad (92)$$

The charge continuity equation in the steady state further gives $J_D = I_1 = -I_N$. The above equation leads to Eq. (17) in the main text. For the intra-bond currents, we choose l at even sites on the wire, i.e., $J_S = J_l$ (even l). This yields :

$$J_S = \frac{I_g}{2} + \frac{\sigma(\delta\mu/e) + I_g l_c/2}{l_c + (N-3)}, \quad (93)$$

which is similar to Eq. (25) in Sec. (IC). Next, we inspect the local thermal equilibrium at the middle sites of the wire. For that, we evaluate the deviation, δn_l , of the local particle density (at any point l) from its corresponding equilibrium density. The local equilibrium density is obtained by imposing the condition: $\mu_{l'} = \mu_l$ for all $l' \in \{1, 2, \dots, N\}$. We obtain the following expression for δn_l in the linear response regime:

$$\begin{aligned} \delta n_l &= \gamma^2 \rho_l(\omega) \sum_{l'=1}^N \int d\omega |G_{ll'}^+(\omega)|^2 [f_{l'}(\omega) - f_l(\omega)] \\ &= \gamma^2 \rho_l(\bar{\mu}) \sum_{l'} |G_{ll'}^+(\bar{\mu})|^2 (\mu_{l'} - \mu_l). \end{aligned} \quad (94)$$

For all points within the bulk of the wire, $G_{ll'}^+(\bar{\mu}) = (-1)^{|l-l'|} e^{-|l-l'|\alpha} / (2 \sinh \alpha)$ for $N \rightarrow \infty$. Then, evaluating the

above summation, we obtain

$$\delta n_l = (-1)^{l+1} \frac{I_g}{2e\pi\gamma^2 \rho_l(\bar{\mu})}. \quad (95)$$

We notice that $\delta n_l \neq 0$ as long as $I_g \neq 0$, i.e., the current driven nonequilibrium steady state does not provide local thermal equilibrium within the bulk of the wire.

Heat dissipation: The driven wire dissipates its energy in the form of heat into the baths (Joule heating). We will see how the presence of driving currents I_g affects the heat dissipation. We will particularly look into the heat energy lost per site within the bulk of the wire. For that, we need to calculate the heat current flowing out of the wire from a site l into the bath coupled at that site. It is defined as follows: $h_l = u_l - \mu_l(-I_l)$, where $u_l = i\gamma_l \langle (c_{l+1}^\dagger + c_{l-1}^\dagger) b_1(l) - b_1^\dagger(l)(c_{l+1} + c_{l-1}) \rangle$ denotes the corresponding flow of the energy current. Like before, we will consider a temperature $T \ll \bar{\mu}/K_B$ and retain the first non-zero terms in the series expansion of h_l about $\mu_l = \bar{\mu}$. In this procedure, we get :

$$h_l = \frac{1}{4\pi} \sum_{l'} \mathcal{T}_{ll'} (\mu_{l'} - \mu_l)^2 = \left[\sigma \left(\frac{2\phi}{el_c} \right)^2 + \nabla \frac{I_g^2}{2} \right]. \quad (96)$$

In the above expression, we use Eqs. (85-86) and the following relation:

$$\lim_{(N-l) \rightarrow \infty} \lim_{l \rightarrow \infty} \sum_{l' \neq 1, N} e^{-2\alpha_R |l-l'|} (l-l')^2 = \frac{\cosh \alpha_R}{2(\sinh \alpha_R)^3}. \quad (97)$$

We find the right hand side of Eq. (96) is equal to $[J_S(\mu_{l-1} - \mu_l) + J_D(\mu_l - \mu_{l+1})]/2$. The first term in Eq.(96) falls as $1/N^2$ (for $N \gg l_c$) as we increase the size of the wire (the diffusive component). We further notice that the nonreciprocal charge current affects only the first term in h_l . The second term in h_l is N -independent. For a fixed $\delta\mu$, such a term in h_l causes the overall heat dissipation in the wire to grow proportional to N . This is not surprising since the uniform driving along the wire will eventually cause more heating. For smaller values of $\gamma \ll 1$, we get

$$h_l \approx \frac{1}{\sigma} \left[\left(\frac{2\phi\sigma}{el_c} \right)^2 + l_c^2 \frac{I_g^2}{4} \right], \quad (98)$$

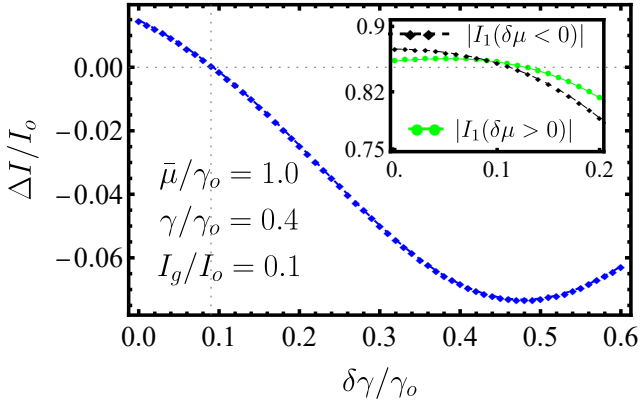


FIG. 3: The variation of the current nonreciprocity with $\delta\gamma$ in a single S-D dimer. We fix $\delta\mu/\gamma_0 = 0.1$ and $e = 1$.

where $\sigma^{-1} \approx 2\pi/(e^2 l_c)$, and $l_c \approx 2/\gamma^2$.

E. Role of contact scattering on current nonreciprocity

Previously, we have chosen $\gamma_l/\gamma_0 = \gamma_N/\gamma_0 = 1$ for the analytical simplicity within the linear response regime. In this subsection, we will consider imperfect contacts between the wire and the L, R-baths, i.e., $\gamma_l/\gamma_0 = \gamma_N/\gamma_0 \neq 1$. This induces contact scattering at the boundaries, which influences the non-reciprocal current transport through the wire.

We first take up a single S-D dimer ($N_i/2 = 1$). In Fig.3, we have shown that the non-reciprocity $\Delta I = |I_1(\delta\mu < 0)| - |I_1(\delta\mu > 0)|$ value gradually decreases to zero with increasing $\delta\gamma$, where $\delta\gamma = \gamma_l - \gamma_0 = \gamma_N - \gamma_0$. Beyond this point, if we further increase $\delta\gamma$, the current flowing in the forward bias $I_1(\delta\mu > 0)$ becomes more than that of flowing in the reverse bias (inset of the Fig. 3). Next, we take $N_i/2 = N/2 - 1$ pairs of S-D dimers in the wire. In Fig.4, we display the variation in ΔI with increasing N for different values of $\delta\gamma$. For a sufficiently long wire, i.e., $N \gg l_c$, we notice ΔI asymptotically approaches I_g , irrespective of the value of $\delta\gamma$. In the intermediate length scales ($N \gtrsim l_c$), ΔI is more for a given N with smaller $\delta\gamma$. Based on this observation, we infer that the introduction of contact scattering effectively enhances the scattering length scale l_c in the quantum wire. The interplay of quantum coherence becomes more prominent for fewer S-D baths $N_i \sim 2$. We notice the oscillatory rise of ΔI from negative values in smaller wire sizes, which can further lead to reciprocal charge transport ($\Delta I = 0$) for a given $N \gtrsim 4$.

III. INTERPLAY BETWEEN QUANTUM COHERENCE AND NONRECIPROCAL CHARGE TRANSPORT

In the previous section, we observe how contact scattering can significantly affect the nonreciprocal current behavior in a short quantum wire. In this section, we will study the special limit of a single S-D dimer in a long wire, which can give reciprocal charge transport. We couple one S and D bath

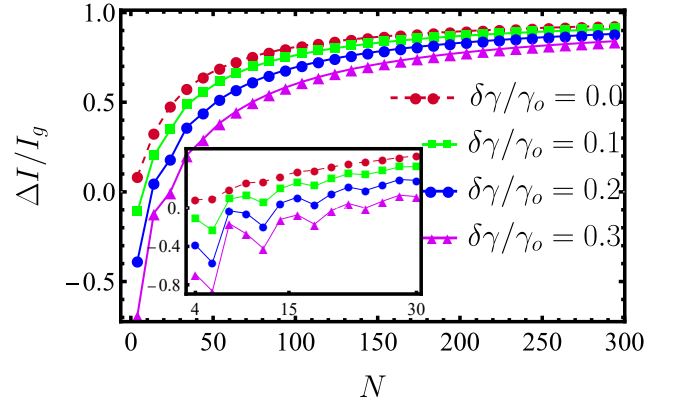


FIG. 4: Nonreciprocity in the charge current vs N for different values of $\delta\gamma$ with multiple S-D dimers. Parameters of the plot are $\bar{\mu}/\gamma_0 = 1.0$, $\delta\mu/\gamma_0 = 0.1$, $\gamma/\gamma_0 = 0.3$, $I_g/I_0 = 0.05$, and $e = 1$.

to the wire at sites $l = 2, N - 1$, respectively. Therefore, we have $\gamma_l = (\delta_{l,2} + \delta_{l,N-1})\gamma$ for $l = 2, 3, \dots, N - 1$. Once again, we fix the couplings at end contacts by $\gamma_l/\gamma_0 = \gamma_N/\gamma_0 = 1$. In the following Subsection. III A, we derive analytical expressions for the chemical potentials of the middle baths and the charge current I_1 across the wire. In the Subsection. III B, we will compare the results with a corresponding setup within the master equation description.

A. Quantum modeling in linear response regime

The S-D currents give the following two equations, which fix μ_2 and μ_{N-1} self-consistently:

$$2\pi(I_g/e) = (\mathcal{T}_{21} + \mathcal{T}_{2N-1} + \mathcal{T}_{2N})\delta\mu_2 - \mathcal{T}_{2N-1}\delta\mu_{N-1} - (\mathcal{T}_{21} - \mathcal{T}_{2N})\delta\mu_L, \quad (99)$$

$$-2\pi(I_g/e) = (\mathcal{T}_{1N-1} + \mathcal{T}_{2N-1} + \mathcal{T}_{NN-1})\delta\mu_{N-1} - \mathcal{T}_{2N-1}\delta\mu_2 - (\mathcal{T}_{1N-1} - \mathcal{T}_{NN-1})\delta\mu_L. \quad (100)$$

We use the following relations: $\mathcal{T}_{l'l'} = \mathcal{T}_{l'l}$, $\mathcal{T}_{12} = \mathcal{T}_{NN-1}$ and $\mathcal{T}_{1N-1} = \mathcal{T}_{2N}$, which immediately give $\delta\mu_2 = -\delta\mu_{N-1} = \Delta\mu_{\mu,N}$. From Eq.(99), we obtain:

$$\Delta\mu_{\mu,N} = \frac{2\pi(I_g/e) + (\mathcal{T}_{21} - \mathcal{T}_{2N})\delta\mu/2}{\mathcal{T}_{21} + 2\mathcal{T}_{2N-1} + \mathcal{T}_{2N}}. \quad (101)$$

The current flowing in the wire can be written as:

$$I_1 = e \frac{(\mathcal{T}_{12} + \mathcal{T}_{1N-1} + 2\mathcal{T}_{1N})\delta\mu_L - (\mathcal{T}_{12} - \mathcal{T}_{1N-1})\Delta\mu_{\mu,N}}{2\pi},$$

which yields : $I_1 = \tilde{G}_N(\delta\mu/e) - \Delta j/2$, where

$$\tilde{G}_N = e^2 \frac{(\mathcal{T}_{12} + 2\mathcal{T}_{1N} + \mathcal{T}_{1N-1})(\mathcal{T}_{21} + 2\mathcal{T}_{2N-1} + \mathcal{T}_{2N}) - (\mathcal{T}_{12} - \mathcal{T}_{1N-1})(\mathcal{T}_{21} - \mathcal{T}_{2N})}{4\pi(\mathcal{T}_{21} + 2\mathcal{T}_{2N-1} + \mathcal{T}_{2N})}, \quad (102)$$

$$\Delta j = 2 \frac{\mathcal{T}_{12} - \mathcal{T}_{1N-1}}{\mathcal{T}_{21} + 2\mathcal{T}_{2N-1} + \mathcal{T}_{2N}} I_g.$$

We only need to evaluate the following four transmission coefficients: $\mathcal{T}_{21}, \mathcal{T}_{N-11}, \mathcal{T}_{N1}$ and \mathcal{T}_{N-12} . The retarded Green's function elements are given by

$$G_{ll'}^+(\bar{\mu}) = \frac{(-1)^{l+l'}}{|\det(\hat{Z})|} (\text{Cofact}[\hat{Z}])_{ll'}, \quad (103)$$

where $\text{Cofact}[\hat{Z}]$ generates the cofactor of the matrix \hat{Z} . \hat{Z} forms a tri-diagonal matrix in real space basis as follows:

$$Z_{ll'} = \begin{pmatrix} A & 1 & 0 & 0 & 0 & \dots & 0 & 0 & 0 \\ 1 & 2D & 1 & 0 & 0 & \dots & 0 & 0 & 0 \\ 0 & 1 & \bar{\mu} & 1 & 0 & \dots & 0 & 0 & 0 \\ 0 & 0 & 1 & \bar{\mu} & 1 & \dots & 0 & 0 & 0 \\ \dots & \dots & \dots & \dots & \dots & \dots & \dots & \dots & \dots \\ 0 & 0 & 0 & 0 & 0 & \dots & \bar{\mu} & 1 & 0 \\ 0 & 0 & 0 & 0 & 0 & \dots & 1 & 2D & 1 \\ 0 & 0 & 0 & 0 & 0 & \dots & 0 & 1 & A \end{pmatrix}_{N \times N}. \quad (104)$$

The determinant of the matrix \hat{Z} is given by

$$\det(\hat{Z}) = (2AD - 1) \{A(2DY_{N-4} - Y_{N-5}) - Y_{N-4}\} - A \{A(2DY_{N-5} - Y_{N-6}) - Y_{N-5}\}, \quad (105)$$

where $A = \bar{\mu}/2 + i\sqrt{1 - \bar{\mu}^4}/4$, $2D = \bar{\mu} - \gamma^2(\bar{\mu} - i\sqrt{4 - \bar{\mu}^2})/2$, and $Y_N = \sin(N+1)k_F/\sin k_F$. Here, k_F denotes the Fermi momentum and is defined via $k_F = \cos^{-1}(\bar{\mu}/2)$. After evaluating the co-factors, we get the required Green's function elements as follows:

$$G_{21}^+(\bar{\mu}) = -\frac{1}{\det(\hat{Z})} \{A(2DY_{N-4} - Y_{N-5}) - Y_{N-4}\}, \quad (106)$$

$$G_{N1}^+(\bar{\mu}) = \frac{(-1)^{N+1}}{\det(\hat{Z})}, \quad G_{N-11}^+(\bar{\mu}) = \frac{(-1)^N}{\det(\hat{Z})} A \quad (107)$$

$$G_{N-12}^+(\bar{\mu}) = \frac{(-1)^{N+1}}{\det(\hat{Z})} A^2. \quad (108)$$

The corresponding transmission coefficients are

$$\mathcal{T}_{21} = \gamma^2 \frac{(4 - \bar{\mu}^2)}{|\det(\hat{Z})|^2} \Xi, \quad \mathcal{T}_{N-11} = \gamma^2 \frac{(4 - \bar{\mu}^2)}{|\det(\hat{Z})|^2}, \quad (109)$$

$$\mathcal{T}_{N1} = \frac{(4 - \bar{\mu}^2)}{|\det(\hat{Z})|^2}, \quad \mathcal{T}_{N-12} = \gamma^4 \frac{(4 - \bar{\mu}^2)}{|\det(\hat{Z})|^2}, \quad (110)$$

where Ξ is an oscillating function of N , and defined by the following relation $\Xi = |A(2D \sin(N-3)k_F - \sin(N-4)k_F) - \sin(N-3)k_F|^2 / \sin^2 k_F$. Utilizing these expressions, we finally get $\Delta_{\mu,N}$, \tilde{G}_N and Δj as follows :

$$\Delta_{\mu,N} = \frac{2\pi |\det(\hat{Z})|^2 I_g / [e(4 - \bar{\mu}^2)\gamma^2] + (\Xi - 1)\delta\mu/2}{\Xi + 1 + 2\gamma^2},$$

$$\tilde{G}_N = \frac{e^2(4 - \bar{\mu}^2)(\gamma^2\Xi + \gamma^2 + 2)(\Xi + 1 + 2\gamma^2) - \gamma^2(\Xi - 1)^2}{|\det(\hat{Z})|^2 4\pi(2\gamma^2 + \Xi + 1)},$$

$$\Delta j = 2 \frac{\Xi - 1}{\Xi + 1 + 2\gamma^2} I_g. \quad (111)$$

Eq. (111) gives the periodic variation of Δj with the system size N , which is displayed in Fig. 2(c) of the main article. We find that whenever $\sin(N-3)k_F = 0$, we get $\Delta j = 0$ (irrespective of the value of γ), i.e., the nonreciprocity in the electrical current vanishes. In this limit

$$\Delta_{\mu,N} \Big|_{\Xi=1} = \frac{\pi |\det(\hat{Z})|^2 I_g}{e(4 - \bar{\mu}^2)\gamma^2(1 + \gamma^2)}. \quad (112)$$

Therefore, the chemical potentials of the S and D baths are independent of $\delta\mu$. This happens whenever the distance between the S and D baths, i.e., $(N-3)$ matches with an integer multiple of $\lambda_F/2$, where $\lambda_F = 2\pi/\cos^{-1}(\bar{\mu}/2)$. Next, we investigate whether such coherence effects survive in a longer wire (with multiple dimers), where we have an extended ballistic region between consecutive S and D baths. In Fig. 5, we considered a wire of size $N = 60$, where the S-baths are coupled at sites $x = 2, 8, \dots, N-4$ and the D-baths are coupled at sites $x = 5, 11, \dots, N-1$. We vary the average value ($\bar{\mu}$) of the L-R chemical potentials using $\delta\bar{\mu}$ (keeping $\delta\mu$ fixed), where $\bar{\mu} = \gamma_o - \delta\bar{\mu}$. We observe that the current nonreciprocity ΔI for different values of γ becomes zero at $\delta\bar{\mu} = 0.0$ (inset of the Fig. 5).

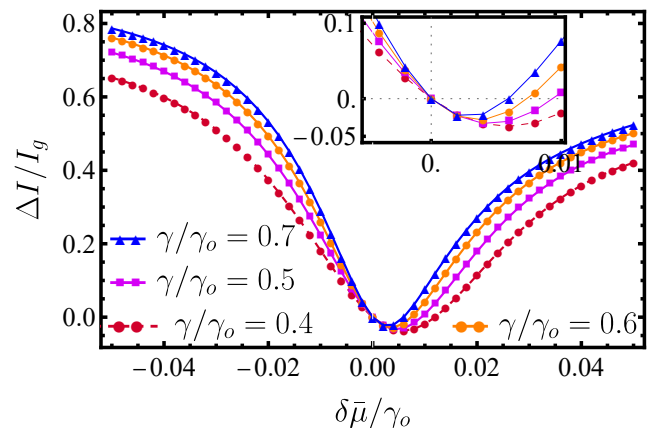


FIG. 5: Control of current nonreciprocity using quantum coherence in a long wire with multiple S-D baths. The parameters are $N = 60$, $\delta\mu/\gamma_o = 0.1$, and $I_g/I_o = 0.1$. We fix $e = 1$ in the plots.

B. Change transport through an extended lattice with one S and D bath using master equation approach

Here, we will show that the oscillations and zeros of current nonreciprocity obtained within the quantum modeling do not appear within the master equation description. We consider a lattice of size $N > 4$. The discrete time-evolution equations for the density fields $\rho^\pm(x, t)$ at the middle sites of the lattice,

with only one S at $x = 2a$ and one D at $x = (N - 1)a$, are:

$$\rho^\pm(2a, t + \tau) - \rho^\pm(2a, t) = \rho^\pm(2a \mp a, t) + (1 - p)\rho^\mp(2a, t) - \rho^\pm(2a, t) + \frac{I_g \tau}{2ae}, \quad (113)$$

$$\rho^+(x, t + \tau) - \rho^+(x, t) = [1 + (p - 1)\delta_{x, 3a}]\rho^+(x - a, t) - \rho^+(x, t), \quad (114)$$

$$\rho^-(x, t + \tau) - \rho^-(x, t) = [1 + (p - 1)\delta_{x, (N-2)a}]\rho^-(x + a, t) - \rho^-(x, t), \quad (115)$$

$$\rho^\pm(L, t + \tau) - \rho^\pm(L, t) = \rho^\pm(L \mp a, t) + (1 - p)\rho^\mp(L, t) - \rho^\pm(L, t) - \frac{I_g \tau}{2ae}, \quad (116)$$

where, $x = 3a, 3a, \dots, (N - 2)a$. The solutions in the steady state are obtained with the boundary condition $\rho^+(a) = \delta\rho + \rho_o$ and $\rho^-(L + a) = \rho_o$, and they are given by

$$\rho^+(2a) = \frac{(2 - p)[\frac{I_g}{2ev_F} + \delta\rho] + (3 - 2p)\rho_o}{p(3 - 2p)}, \quad (117)$$

$$\rho^-(2a) = \frac{\rho_o + 2(1 - p)[\frac{I_g}{2ev_F} + \delta\rho + \rho_o]}{p(3 - 2p)}, \quad (118)$$

$$\rho^+(L) = \frac{(p - 1)\frac{I_g}{ev_F} + \delta\rho + (3 - 2p)\rho_o}{p(3 - 2p)}, \quad (119)$$

$$\rho^-(L) = \frac{(p - 2)\frac{I_g}{2ev_F} + (1 - p)\delta\rho + (3 - 2p)\rho_o}{p(3 - 2p)}. \quad (120)$$

The rest is obtained using: $\rho^+(L - a) = \rho^+(L - 2a) = \dots = \rho^+(3a) = p\rho^+(2a)$, and $\rho^-(3a) = \rho^-(4a) = \dots = \rho^-(L - a) = p\rho^-(L)$. Therefore, the current entering (leaving) the lattice is

$$I_{\text{in}} = I_{\text{out}} = \frac{ev_F \delta\rho - (1 - p)I_g}{3 - 2p}, \quad (121)$$

and the current in the lattice between the S and D is

$$J(x) = \frac{ev_F \delta\rho + (2 - p)I_g}{3 - 2p}, \quad x = 2a, 3a, \dots, L - a. \quad (122)$$

We found that the current propagating through the lattice is independent of its length, and consequently, the nonreciprocity does not vary with N .

IV. RESISTIVE CIRCUIT MODEL OF MULTIPLE S-D DIMERS

In the main article, we motivated our introduction with a single S and D current in a resistive circuit. Here, we focus on the resistive circuit model of the wire (length L) coupled to multiple S and D currents. Let us assume there are $N_i/2 = \tilde{N}/2 - 1$ pairs of S and D currents arranged in the configuration (SDSD...) on the wire with a separation \tilde{a} between them. The resistance R of the wire is uniformly distributed along its length, i.e., $R = L/\sigma$, where σ denotes the wire's

conductivity. All the currents are taken due to the flow of positive charges ($e > 0$). The current flowing into the wire for a forward voltage bias V is

$$I_{\text{in}} = \frac{\sigma V - (\tilde{N}/2 - 1)\tilde{a}I_g}{(\tilde{N} - 1)\tilde{a}} = \sigma \frac{V}{L} - \frac{I_g}{2} \left(1 - \frac{\tilde{a}}{L}\right). \quad (123)$$

Next, we provide the voltage drop $V(x)$ at the locations x in the wire where the S and D currents are coupled:

$$V(l\tilde{a}) = V - \frac{\tilde{a}}{L} \left(V + \frac{I_g \tilde{a}}{2\sigma} \right) (l - 2) - \frac{\tilde{a}}{L} \left(V - \frac{I_g L - 2\tilde{a}}{4\sigma} \right) + (-1)^l \frac{I_g}{4} \left(\frac{\tilde{a}}{\sigma} \right), \quad \text{for } l = 2, 3, \dots, \tilde{N} - 1. \quad (124)$$

The voltage bias across the boundaries give $V(\tilde{a}) = V$, and $V(L + \tilde{a}) = 0$. Now, the heat evolved per unit time from the wire (Joule heating) due to the flow of charges between sites $x = l\tilde{a}$ and $x = (l + 1)\tilde{a}$ is :

$$\tilde{h}_{l, l+1} = \frac{\tilde{a}}{\sigma} \left[\frac{\sigma V + \tilde{a}I_g/2}{L} + (-1)^l \frac{I_g}{2} \right]^2. \quad (125)$$

Therefore, the average heat energy generated (per unit time) from the bulk of the wire, over a length scale \tilde{a} , is :

$$\frac{\tilde{h}_{l-1, l} + h_{l, l+1}}{2} = \frac{\tilde{a}}{\sigma} \left[\left(\frac{\sigma V + \tilde{a}I_g/2}{L} \right)^2 + \left(\frac{I_g}{2} \right)^2 \right]. \quad (126)$$

The above expression resembles the form obtained using the microscopic treatment in Eq. (96).

A. Correspondence between the resistive and the master equation descriptions of multiple S-D dimers

Let us now consider a large number of S-D currents coupled to the circuit, such that $\tilde{a}/L = (\tilde{N} - 1)^{-1} \equiv \mathcal{O}(1/\tilde{N}) \rightarrow 0$. In this limit, we rewrite $V(x)$ as follows:

$$V(l\tilde{a}) = V \left(1 + \frac{\tilde{a}}{L} \right) - \left(V + \frac{I_g \tilde{a}}{2\sigma} \right) \frac{\tilde{a}l}{L} + \frac{I_g}{4} \left(\frac{\tilde{a}}{\sigma} \right) \left(1 + 2\frac{\tilde{a}}{L} \right) + (-1)^l \frac{I_g}{4} \left(\frac{\tilde{a}}{\sigma} \right) \approx V - \left(V + \frac{I_g \tilde{a}}{2\sigma} \right) \frac{\tilde{a}l}{L} + [1 + (-1)^l] \frac{I_g}{4} \left(\frac{\tilde{a}}{\sigma} \right), \quad (127)$$

for $l = 2, \dots, \tilde{N} - 1$. Here, in the large \tilde{N} limit, we have neglected the terms V/\tilde{N} , $I_g \tilde{a}/(\sigma \tilde{N})$ in comparison to the others are already present. The resistive model does not have a coherence length scale that allows the ballistic charge transport for a finite voltage bias V . Therefore, to draw a comparison between the resistive and the master equation descriptions, we consider the thermodynamic limit ($N \rightarrow \infty$) on the corresponding lattice model introduced in Sec. I, such that $L \gg l_c$. The total density of particles at the middle sites of the lattice becomes

$$\rho^+(x) + \rho^-(x) \approx 2(\rho_o + \delta\rho) - \left(2\delta\rho + \frac{I_g}{2} \frac{2}{ev_F} \right) \frac{x}{L} + [1 + (-1)^{\frac{x}{\tilde{a}}}] \frac{I_g}{4} \frac{2}{ev_F}, \quad (128)$$

for $x = 2a, 3a, \dots, L$. In this limit, we can rewrite the current entering the lattice as follows:

$$I_{\text{in}} \approx \frac{ev_F \delta \rho l_c}{L} - \frac{I_g}{2} \left(1 - \frac{l_c}{L}\right). \quad (129)$$

For a given length L of the circuit wire (and the lattice), if we identify the coordinate x on the lattice with the distance $l\tilde{a}$ on the circuit, then

$$V(l\tilde{a}) - V \equiv K \left[\rho^+(x) + \rho^-(x) - 2(\rho_o + \delta\rho) \right], \quad (130)$$

such that :

$$L = Na \equiv \tilde{N}\tilde{a}, \quad V \equiv K(2\delta\rho), \quad \text{and} \quad \frac{\sigma}{\tilde{a}} \equiv \frac{1}{K} \frac{ev_F}{2}. \quad (131)$$

The above expressions give $\sigma V/\tilde{a} \equiv ev_F \delta\rho$. On the other hand, comparing the first term of the incoming current I_{in} in Eqs. (123, 129), we get: $\sigma V \equiv ev_F \delta\rho l_c$. Therefore, we estab-

lish a correspondence between the two models by identifying

$$\tilde{a} \equiv l_c = \frac{a}{1-p}. \quad (132)$$

This identification signifies a coarse-graining on the length scales: $(N/2 - 1)$ pairs of S-D dimers on the lattice model correspond to $(\tilde{N}/2 - 1)$ pairs of S and D currents in the circuit model, where $\tilde{N} \equiv (a/l_c)N$.

We now focus on the following expression:

$$\sigma V \equiv ev_F \delta\rho l_c = \left[\frac{e^2 \rho_{\text{av}}}{m_e} \tau_c \right] \left[\frac{m_e (\delta\rho/\rho_{\text{av}}) v_F^2}{e} \right]. \quad (133)$$

On the right-hand side, we introduced the mass of the mobile charges as m_e and $\tau_c = l_c/v_F$. Further, ρ_{av} denotes the average density of the charge carriers inside the lattice. Using the dimensional analysis, we choose $K = m_e v_F^2 / (2e\rho_{\text{av}})$ to identify

$$\sigma \equiv \frac{e^2 \rho_{\text{av}}}{m_e} \tau_c, \quad (134)$$

$$eV \equiv \frac{m_e v_F^2}{2} (2\delta\rho/\rho_{\text{av}}). \quad (135)$$